© 2020. Published by The Company of Biologists Ltd | Development (2020) 147, dev182063. doi:10.1242/dev.182063

STEM CELLS AND REGENERATION

RESEARCH ARTICLE

WD40 protein Wuho controls germline homeostasis via TRIM-NHL tumor suppressor Mei-p26 in *Drosophila*

Elham Rastegari[1,2,3], Kreeti Kajal[3,4,5], Boon-Shing Tan[6], Fu Huang[6], Ruey-Hwa Chen[6], Tao-Shieh Hsieh[1,2,3,*] and Hwei-Jan Hsu[1,2,3,4,5,‡]

ABSTRACT

WD40 proteins control many cellular processes via protein interactions. *Drosophila* Wuho (Wh, a WD40 protein) controls fertility, although the involved mechanisms are unclear. Here, we show that Wh promotion of Mei-p26 (a human TRIM32 ortholog) function maintains ovarian germ cell homeostasis. Wh and Mei-p26 are epistatically linked, with *wh* and *mei-p26* mutants showing nearly identical phenotypes, including germline stem cell (GSC) loss, stem-cyst formation due to incomplete cytokinesis between GSCs and daughter cells, and overproliferation of GSC progeny. Mechanistically, Wh interacts with Mei-p26 in different cellular contexts to induce cell type-specific effects. In GSCs, Wh and Mei-p26 promote BMP stemness signaling for proper GSC division and maintenance. In GSC progeny, Wh and Mei-p26 silence *nanos* translation, downregulate a subset of microRNAs involved in germ cell differentiation and suppress ribosomal biogenesis via dMyc to limit germ cell mitosis. We also found that the human ortholog of Wh (WDR4) interacts with TRIM32 in human cells. Our results show that Wh is a regulator of Mei-p26 in *Drosophila* germ cells and suggest that the WD40-TRIM interaction may also control tissue homeostasis in other stem cell systems.

KEY WORDS: GSC, Stem-cyst, Abscission, Mitosis, Meiosis, BMP, Bam, WDR4

INTRODUCTION

Stem cell self-renewal and differentiation must be balanced for proper tissue homeostasis (Nakada et al., 2011; Simons and Clevers, 2011; Spradling et al., 2011). This balance is known to be coordinated by transcriptional and post-transcriptional mechanisms (Simons and Clevers, 2011; White-Cooper and Caporilli, 2013), which have not been fully described at a molecular level. An excellent model for studying genetic regulation of the cell fate transition from stem cell to differentiated progeny is the *Drosophila* ovary, as its germline stem cells (GSCs) and differentiated progeny are well characterized in cell biology (Fig. 1A,A′) (Wong et al., 2005). Although the physiology of *Drosophila* egg production is well described at a cellular level, the molecular regulatory mechanisms are still an area of active investigation.

Wuho (Wh; meaning 'no progeny' in Chinese) is an evolutionarily conserved protein comprising five WD40 domains (Cheng et al., 2016; Wu et al., 2006), which mediate protein-protein interactions (Xu and Min, 2011). Homologs of Wh have been shown to exert a wide variety of functions via interactions with m7G46 tRNA methyltransferase, Flap endonuclease 1 (FEN1) and Culin-Ring ubiquitin ligase 4 (Alexandrov et al., 2002; Cheng et al., 2016; Wang et al., 2017). Interestingly, *wh* mutant males are sterile because their spermatids are not properly elongated to make functional spermatozoa, and female flies are semi-sterile for unknown reasons (Wu et al., 2006), suggesting that Wh may potentially play an important role in the molecular regulatory circuitry of the GSC lineage.

Interestingly, the ovarian phenotypes we report in Wh mutants are strikingly similar to those in Mei-p26 mutants. Mei-p26 is a member of the tripartite motif and Ncl-1, HT2A and Lin-41 domain (TRIM-NHL) family of proteins, which is highly conserved among metazoans (Sardiello et al., 2008). TRIM-NHL proteins are known to control developmental transitions through mechanisms such as the promotion of stem cell differentiation by suppressing proliferation (Chen et al., 2014). The molecular action of TRIM-NHL proteins is typically ubiquitination and translation silencing via E3 ligase RING domains; meanwhile, the NHL domains mediate protein-protein interactions (Tocchini and Ciosk, 2015). In the *Drosophila* germline, Mei-p26 controls GSC maintenance and differentiation depending on its expression level (Li et al., 2012; Neumüller et al., 2008; Page et al., 2000). However, the regulators of Mei-p26 in the GSC lineage are not known. In this study, we show that Wh is a key regulator of Mei-p26, and that these proteins function together in multiple contexts to control GSC maintenance and differentiation for germline homeostasis. Our results document a potentially generalizable role for WD40 proteins as a bridge between TRIM-NHL proteins and other cellular components, a function that is necessary to balance self-renewal and differentiation in the GSC lineage.

RESULTS

Depletion of *wh* causes germ cell outgrowth and fecundity defects

Wh was suggested to be a modulator of female fly fertility, as females homozygous for the wh^7 null allele produce low numbers of progeny (Wu et al., 2006). However, wh^7 is a truncated mutation generated by imprecise P-element excision, which resulted in the deletion of the *wh* gene as well as the 5′ end of the neighboring *top3β* gene (Fig. 1B). To test whether *wh* deficiency alone is sufficient to produce the fertility defects seen in wh^7 mutant females, we utilized CRISPR/Cas9 to generate a new *wh* null mutant allele, wh^{CRISPR}. In this mutant, a CRISPR cassette containing stop codons and RFPs driven by an eye-specific promoter was inserted 50 to 60 nucleotides after the *wh*

[1]Molecular and Cell Biology, Taiwan International Graduate Program, Academia Sinica, Taipei 11529, Taiwan, R.O.C. [2]Graduate Institute of Life Science, National Defense Medical Center, Taipei 11490, Taiwan, R.O.C. [3]Institute of Cellular and Organismic Biology, Sinica, Taipei 11529, Taiwan, R.O.C. [4]Molecular and Biological Agricultural Sciences Program, Taiwan International Graduate Program, National Chung Hsing University and Academia Sinica, Taipei 11529, Taiwan, R.O.C. [5]Graduate Institute of Biotechnology, National Chung Hsing University, Taichung 40227, Taiwan, R.O.C. [6]Institute of Biological Chemistry, Sinica, Taipei 11529, Taiwan, R.O.C.
*Deceased, August 4, 2016

‡Author for correspondence (cohsu@gate.sinica.edu.tw)

E.R., 0000-0001-5264-3743; K.K., 0000-0001-8816-5747; B.-S.T., 0000-0002-3789-8673; R.-H.C., 0000-0001-8124-5832; H.-J.H., 0000-0001-7892-2310

Received 1 July 2019; Accepted 3 December 2019

Development (2020) 147, dev182063. doi:10.1242/dev.182063

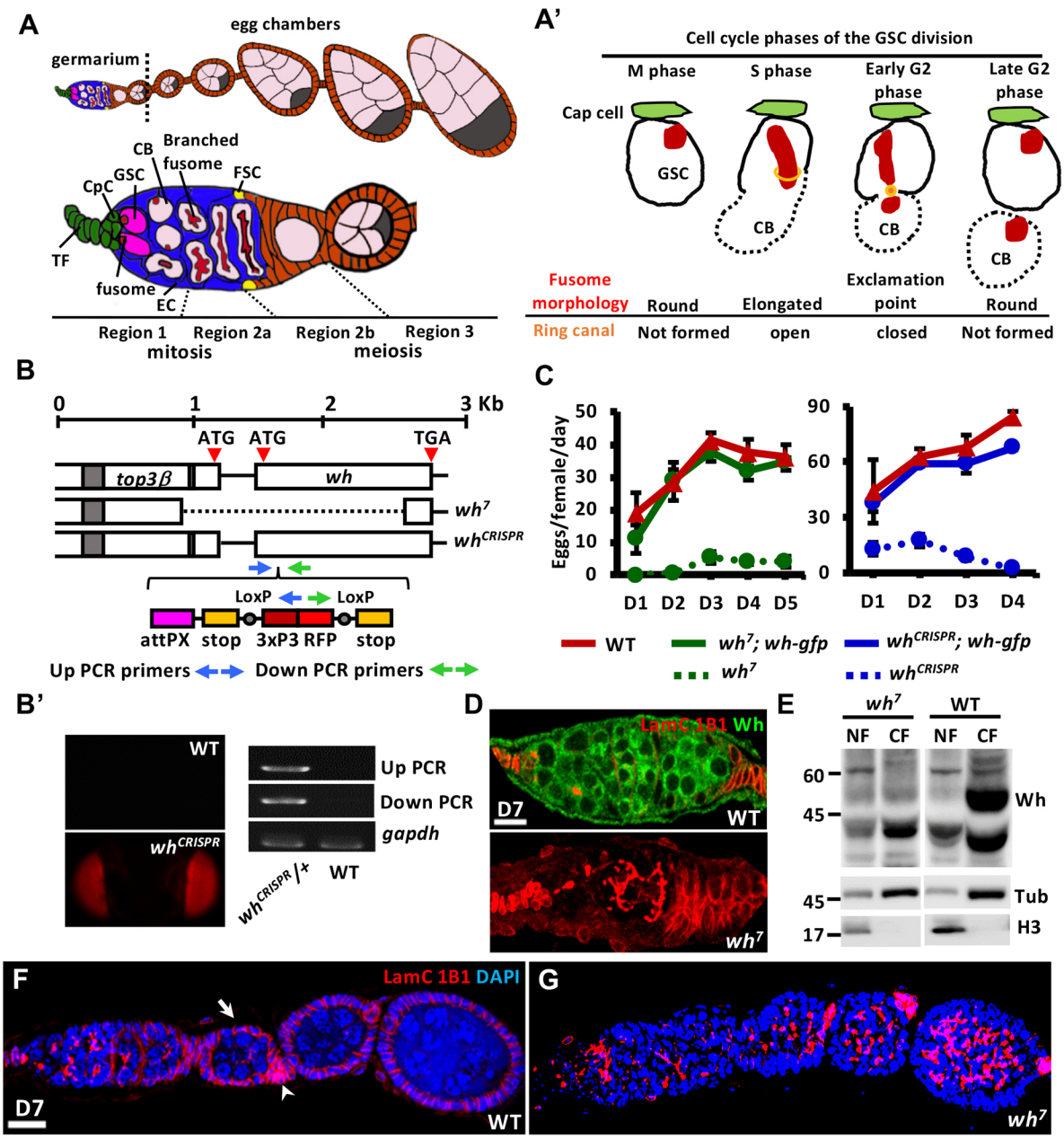

Fig. 1. Wh is mainly located in the cytoplasm of ovarian cells and controls germ cell growth and fecundity. (A) The *Drosophila* ovariole/germarium. The ovariole (Stirnimann et al., 2010) is composed of the germarium in the anterior-most part, followed by a string of progressively older egg chambers. In the germarium (bottom), terminal filament (TF) cells, cap cells (CpCs) and anterior escort cells (ECs) form the germline stem cell (GSC) niche. Each GSC carries a cytoplasmic organelle, called the fusome. The GSC progeny cystoblast (CB) undergoes four rounds of incomplete mitotic division within regions 1 and 2a to form a 16-cell cyst. Each cell in the cyst is interconnected by a branched fusome. In region 2b, the germ cell cyst undergoes meiosis, changing to a lens-shaped cyst and acquiring a monolayer of follicle cells derived from follicle stem cells (FSCs). In region 3, a round germ cell cyst completely surrounded by follicle cells buds off from the germarium as an egg chamber, in which the fusome is degraded. (A′) The GSC complete abscission. At M phase, the GSC (solid line) carries a round-shaped fusome (red). After mitosis, the GSC is still connected with its daughter cell, the CB (dashed line), and the GSC fusome is elongated to fuse with the nascent fusome that is formed within the ring canal of the CB at S phase. At early G2 phase, the ring canal is closed and partitions the fusome, creating an 'exclamation point' morphology. At late G2 phase, the GSC completely separates from the CB, and the fusome returns to its round shape after the ring canal is closed. (B) The genomic structure of the *wh* gene and its mutants. wh^{7}, generated by P-element excision, has a 1426-bp deletion covering the coding region of *wh* and the 5′ end of the neighboring *top3β* gene. wh^{CRISPR} has a deletion of 50-60 bp after the *wh* gene start codon, and replacement of a CRISPR cassette with an attPX site, 3-frame stop codon and floxed 3× P3-RFP leading to RFP expression in the eyes. (B′) Knock-in of the CRISPR cassette was validated by the presence of RFP signal in the eyes of wh^{CRISPR} mutant flies, and by genomic PCR using two primer pairs given in B (Table S1). (C) The egg production per female per day (D1-D5) of indicated genotype; data are mean±s.d. (D) Seven-day-old wild-type (WT) and wh^{7} mutant germaria with 1B1 (red, fusomes), LamC (red, TF and CpC nuclear envelopes), Wh (green) and DAPI (gray, DNA). (E) Representative immunoblot shows that Wh is mainly present in the cytosolic fraction of wild-type ovary extracts. Histone (H3) and beta-tubulin (Tub) were used as nuclear and cytoplasmic markers, respectively. wh^{7} mutant ovaries were used as a negative control. (F,G) 3D-reconstructed images of 7-day-old wild-type (WT) (F) and wh^{7} mutant germaria (G) showing 1B1 (red, fusomes and membranes of follicle and stalk cells, which links two egg chambers), LamC (red) and DAPI (blue). Arrow and arrowheads point to follicle cells and stalk cells, respectively. Genotype of wild-type in B′,C,D,E and F is w^{1118}. Scale bar: 10 µm.

Development (2020) 147, dev182063. doi:10.1242/dev.182063

transcriptional start site (Fig. 1B). wh^{CRISPR} and wh^{7} mutant females exhibited similarly dramatic reductions in egg laying when compared with controls or *wh* mutants bearing a wild-type *wh* transgene (Fig. 1C), suggesting a role for Wh in fecundity control.

To understand how Wh affects egg production, we first generated antibodies for western blot (see Materials and Methods) and for immunofluorescence (antibody generated by T.-S.H.), and examined Wh expression in the ovary. Wh was highly expressed and localized in the cytoplasm of nearly all germ cells and somatic cells (Fig. 1D,E), but was absent from the *wh* mutant, demonstrating the specificity of the anti-Wh antibody. We also examined the cell compositions in *wh* mutant ovarioles by labeling fusomes (Fig. 1F,G) (Lin et al., 1994) with 1B1 antibody against Hu-li tai shao, an Adducin-like protein (Zaccai and Lipshitz, 1996). In the wild-type ovariole (Fig. 1F), fusomes were only present in the germarium; GSCs and cystoblasts (CBs) contained round-shaped fusomes, whereas germ-cell cysts carried a branched fusome. In contrast, nearly 70% of wh^{7} mutant ovarioles (more than hundreds of ovarioles were examined) exhibited highly branched fusomes mislocalized in the germarium and egg chambers (Fig. 1G). Given that fusomes grow during germ cell division (McKearin, 1997; Storto and King, 1989), these data suggest that *wh* deletion results in overproliferation of germ cells and coincident fecundity defects.

Wh cell-autonomously controls maintenance and abscission of female GSCs as well as synchronous division of progeny

To investigate whether Wh controls germ cell homeostasis, we examined GSC number in wh^{7} mutant germaria by counting the number of fusomes adjacent to niche cap cells with nuclear envelopes labeled by LamC (Hsu and Drummond-Barbosa, 2009). We found that wh^{7} mutant germaria carried fewer GSCs and the number further decreased with age (Fig. 2A,B,G), whereas niche cap cell numbers remained comparable with those in wild-type germaria (Fig. S1). The completion of cytokinesis between GSCs and CBs was marked by closure of the ring canal and the exclamation point morphology of the GSC fusome (Fig. 2C; see also Fig. 1A′) (Hsu et al., 2008; Kao et al., 2015). Strikingly, 67±6% (mean±s.d.) of wh^{7} mutant germaria (n=250) carried GSCs that were connected to several daughter cells via long branched fusomes with open ring canals between cells, forming stem-cysts (Fig. 2B,D,H). The number of wh^{7} mutant germaria with stem-cysts increased with age (Fig. 2G). As expected, the wild-type CB underwent four rounds of incomplete division to sequentially become a 2-, 4-, 8- and then 16-cell cyst (see insets in Fig. 2A), and cells in the 8-cell cyst were synchronous in terms of cell cycle progression (Fig. 2E,E′), according to the level of BrdU signal (S phase marker) in germ cells. In contrast, germ cells in the wh^{7} stem-cyst were asynchronous, as not all germ cells within an 8-cell cyst were positive for BrdU incorporation (Fig. 2F,F′). Further, the largest cyst size in wild-type germaria was always 16 cells, whereas the cyst size in wh^{7} mutant germaria varied. In some cases, stem-cysts in the mutant contained odd numbers of cells and/or the cysts had more than 16 cells (Fig. 2I), indicating a loss of the 2^{n} rule for germ cell division.

To further examine the requirement for Wh in germ cell homeostasis, we disrupted *wh* expression specifically in the germline using an *RNAi* line driven by the *nanos (nos)-GAL4* germ cell driver (Rørth, 1998). Wh expression was undetectable in germline cells of $nos{>}wh^{RNAi}$ germaria (Fig. 2J,K), indicating high efficiency knockdown in the wh^{RNAi} line. As expected, GSCs were dramatically reduced and stem-cysts were present in 77.7% of $nos{>}wh^{RNAi}$ germaria (n=53) (Fig. 2L-N). Similar results were also obtained from a clonal analysis (Fig. S2), wherein GSCs with the wh^{7} or wh^{CRISPR} homozygous mutation induced by the Flipase/Flipase recognition target system exhibited poor maintenance (Fig. S5A,B,E), formed stem-cysts (Fig. S2D) and progeny did not follow the 2^{n} rule (Fig. S2B,C). These results indicate that Wh controls GSC maintenance and abscission, as well as synchronous division of germ cells in a cell-autonomous manner.

wh mutant germ cells are defective in mitosis exit and meiosis entry

Because massive branched fusomes occupied the entire *wh* mutant germarium and were also present in early egg chambers (Fig. 1E and Fig. 2), we hypothesized that *wh* mutant germ cells may not properly exit mitosis and initiate meiosis. To test this idea, we examined expression patterns of several mitotic markers in *wh* mutant germaria: phospho-Histone H3 (PHH3) labeled M phase, BrdU labeled S phase and Cyclin B (CycB) labeled G2 and M phases (Hsu et al., 2008; Kao et al., 2015). In the wild type (Fig. 3A), 22% and 68% of germaria (n=50) carried PHH3- and BrdU-positive germ cells, respectively. These positively stained germ cells were mitotic and present in regions 1 (PHH3- and BrdU-positive germ cells) and 2a (BrdU-positive germ cells), but not in region 3, in which germ cells undergo meiosis (Lin and Spradling, 1993; Wettstein and Sotelo, 1971). In contrast, 50% and 91% of wh^{7} mutant germaria (n=64) carried PHH3- or BrdU-positive germ cells, respectively, with mitotic germ cells present in the posterior region. Note that *wh* mutant germaria were not able to be defined into three regions as they had abnormal cell arrangement and structure (Fig. 3B). Similar phenomena were also observed in germaria labeled with CycB (Fig. 3C,D) and γ-tubulin (Fig. 3E,F), which labels centrosomes that mark the onset of mitosis (Khodjakov and Rieder, 1999). These results indicate that wh^{7} mutant germ cells are mitotically active and persist in mitosis.

We further examined whether wh^{7} mutant germ cells underwent meiosis by labeling C3G, a component of the synaptonemal complex formed at the onset of meiosis (Page and Hawley, 2001), and γ-H2Av, a marker for double strand breaks (DSBs) that are induced during meiosis (Jang et al., 2003). As described in previous reports, meiosis was initiated in the early 16-cell cyst at region 2a, with small punctate C3G foci corresponding to the zygotene stage of meiosis (Page and Hawley, 2001). However, the zygotene stage is too brief to be observed in every germarium (Manheim and McKim, 2003). In agreement with these reports, C3G expression in the wild-type germarium was concentrated in two germ cells (pro-oocytes at pachytene of meiotic prophase I) of the lens-shaped 16-cell cyst, and only present in the oocyte of the egg chamber (Fig. 3G,G′). On the other hand, γ-H2AV foci were observable in region 2a/b but absent in the late region 2b of the wild-type germarium (Fig. 3G), suggesting that DSBs are repaired as meiosis proceeds (Hughes et al., 2018). In contrast, 40% of wh^{7} mutant germaria (n=83) were negative for both C3G and γH2AV (Fig. 3H). Perhaps the germ cells in these germaria did not enter meiosis or the 16-cell cyst stage was not reached. Nevertheless, ∼25% of wh^{7} mutant germaria carried germ cell cysts with punctate expression of C3G (Fig. 3I,I′), suggesting that some germ cells may be arrested in the zygotene stage of meiosis. About 30% of wh^{7} mutant germaria showed one or more large γ-H2Av foci (Fig. 3J), indicating DNA damage (Kuo and Yang, 2008; Lake et al., 2013). Consistent with these findings, we also saw that ∼30% of wh^{7} mutant germaria carried apoptotic germ cells (Fig. S3). Notably, these phenotypes – massive branched fusomes, stem-cysts, meiosis failure and germ cell death – were also observed in wh^{CRISPR} mutant germaria (Fig. S4). As a consequence, formation of oocytes [marked by Orb; Lantz et al., 1994] was disrupted (indicated by Orb not being specified to a single germ cell at a right gradient) in 24% or absent in 66% of wh^{7} mutants (n=60) compared with controls (Fig. 3K-P). It is also

Development (2020) 147, dev182063. doi:10.1242/dev.182063

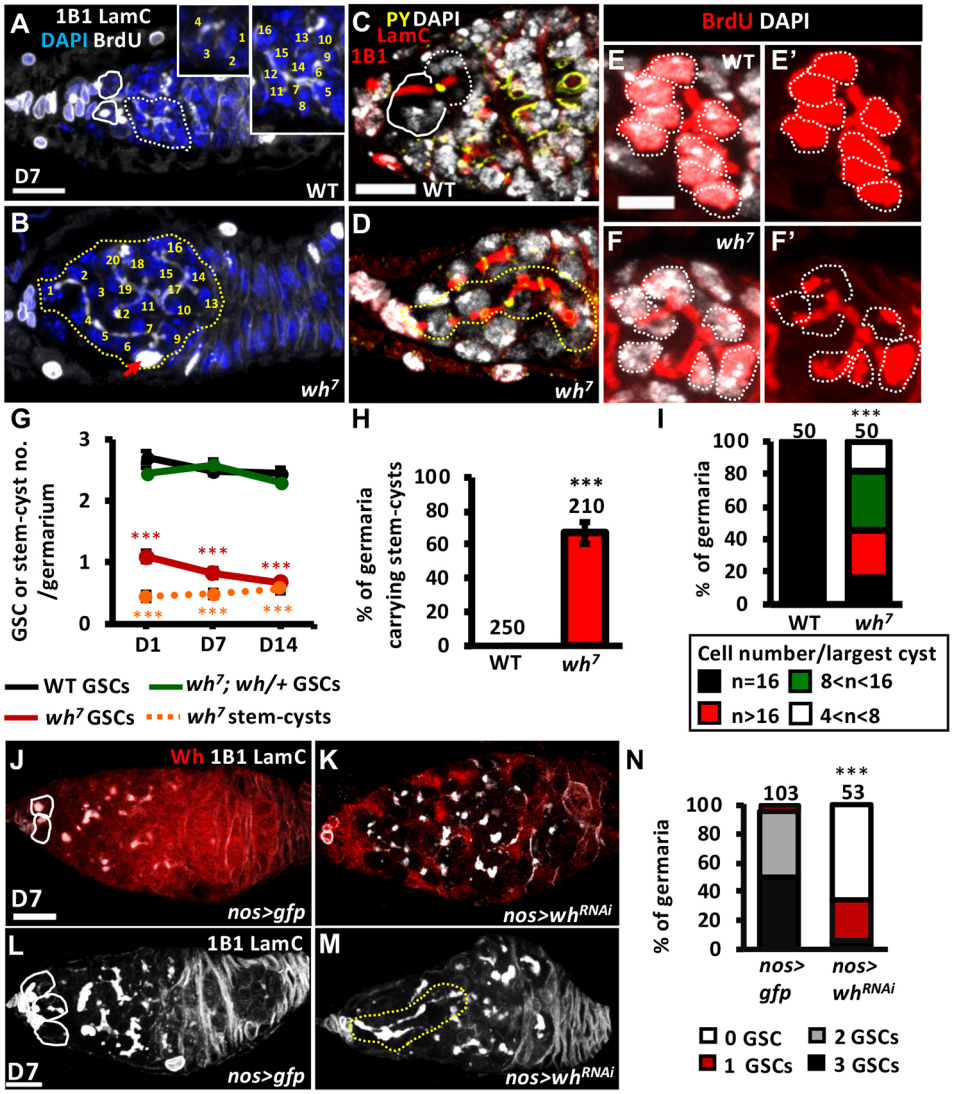

Fig. 2. Wh controls maintenance and abscission of GSCs and synchronous division of GSC progeny in a cell-autonomous manner. (A,B) Wild-type (WT) (A) and *wh*^{7} mutant (B) germaria with 1B1 (gray, fusomes), LamC (gray, terminal filament and cap cell nuclear envelopes), BrdU (gray, S phase marker) and DAPI (blue, DNA). Insets in A are the enlarged view from different focal planes of the 16-cell cyst marked by a dotted line. Arabic numerals show germ cell number in the 16-cell cyst shown in A, and the stem-cyst in B. Note that the stem-cyst in B has 20 germ cells, whereas only one germ cell is positive for BrdU labeling (red arrow), indicating asynchronous division. (C,D) Wild-type (C) and *wh*^{7} mutant (D) germaria showing 1B1 (fusome), LamC (red), phospho-tyrosine [PY] (yellow, ring canals) and DAPI (gray). (E-F′) Wild-type (E) and *wh*^{7} mutant (F) 8-cell cysts showing 1B1 (red), BrdU (red) and DAPI (gray). E′ and F′ show the BrdU channel. (G) Number of GSCs or stem-cysts per germaria in 1-, 7- and 14-day-old (D1, D7 and D14, respectively) flies of indicated genotypes. (H) The percentage of germaria carrying stem-cyst(s) in flies with indicated genotypes. (I) Percentage of germaria with the largest cyst containing indicated germ cell numbers. (J,K) *nos>gfp* (J) and *nos>wh*^{RNAi} germaria (K) showing 1B1 (gray), LamC (gray) and Wh (red). (L,M) *nos>gfp* (L) and *nos>wh*^{RNAi} germaria (M) showing 1B1 (gray), and LamC (gray). (N) Percentage of germaria carrying indicated number of GSCs in flies with indicated genotypes. GSCs are outlined by white solid lines; stem-cysts are outlined by yellow dotted lines; GSC progeny are outlined by white dotted lines. Data in G and H are mean±s.e.m. The stem-cysts in H are compared using two-tailed Student's *t*-test. Numbers of cyst cells (I) and GSCs (N) were compared using a chi-squared test. The numbers above the bars in G,I and N are numbers of analyzed germaria. ***P<0.001. Representative 7-day-old germaria are shown in the 3D-reconstructed images. Genotype of wild-type is *w*^{1118}. Scale bars: 10 µm in A,C,J,L; 5 µm in E.

noteworthy that some *wh* mutant egg chambers showed a tumor-like phenotype, as they contained more than 16 germ cells (Fig. 3O,P), probably because of excessive germ cell mitosis. Thus, at a fundamental level, our results show that Wh is required for proper functioning of germ cell mitosis and meiosis programs.

wh and *mei-p26* mutants exhibit similar phenotypes and Wh interacts with Mei-p26 in the ovary

Surprisingly, we found that the same phenotypes observed in *wh*^{7} mutant germaria, including stem-cysts, germ cell outgrowth with massive branched fusomes and fertility defect, are also present in *mei-p26* mutants, i.e. *mei-p26*^{mfs1}/*mei-p26*^{fs1} (Fig. 4A,B; Table 1) (Li et al., 2012; Neumüller et al., 2008). These similar phenotypes suggest that Wh and Mei-p26 may work in the same pathway to control germ cell homeostasis. To determine whether Wh acts either upstream or downstream of Mei-p26 to affect germ cell homeostasis, we first examined expression of Mei-p26 in *wh* mutant germaria and expression of Wh in *mei-p26* mutant germaria. Mei-p26 expression was present in *wh*^{7} mutant germaria (Fig. 4C,D), and Wh expression levels and patterns were similar in wild-type and

Development (2020) 147, dev182063. doi:10.1242/dev.182063

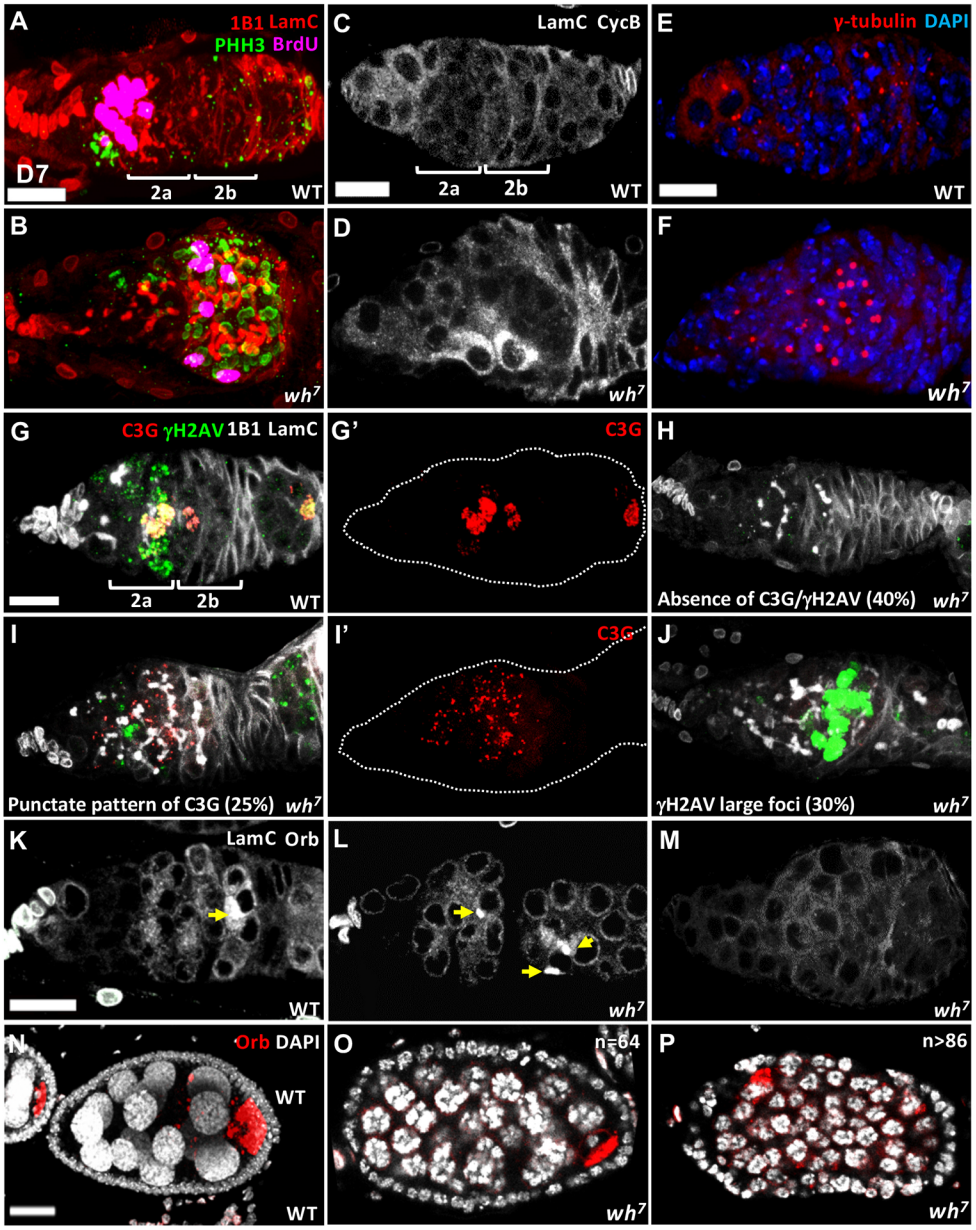

Fig. 3. Wh controls germ cell mitosis exit and meiosis entry. (A-F) Wild-type (A,C,E) and *wh*^{7} mutant (B,D,F) germaria showing 1B1 (red, fusomes), LamC (red, cap cell nuclear envelopes), BrdU (magenta, S phase marker) and PHH3 (green, M phase marker) in A and B, showing LamC (gray) and CycB (gray, G2/M phase marker) in C and D, and showing DAPI (blue, DNA) and γ-tubulin (red, enriched in the centrosome when cells initiate mitosis) in E and F. (G-M) Wild-type (G,K) and *wh*^{7} mutant (H-J,L,M) germaria showing 1B1 (gray), LamC (gray), C3G (red, synaptonemal complex) and γ-H2AV (green, meiosis-induced double strand break) in G-J, showing LamC (gray) and Orb (gray, oocyte marker) in K-M. Yellow arrows in K and L point to Orb-enriched germ cells (oocytes in wild-type). G′ and I′ show only the C3G channel. (N-P) Wild-type (N) and *wh*^{7} mutant (O,P) egg chambers showing DAPI (gray) and Orb (red). Brackets in A,C, and G mark regions 2a and 2b, where mitosis and meiosis, respectively, occur in wild-type flies. *n* is the germ cell number in N and O. The white dotted lines in G′ and I′ mark the periphery of germaria. Representative 7-day-old germaria are shown in 3D-reconstructed images. Genotype of wild-type is *w*^{1118}. Scale bars: 10 µm.

mei-p26 mutant germ cells (Fig. 4E,F). These results suggested that Wh might work with Mei-p26 in the same complex to maintain germ cell homeostasis, as both Wh and Mei-p26 bear protein-protein interaction domains. To test this hypothesis, we used ovaries carrying a *wh-gfp* transgene to perform an immunoprecipitation assay, pulling down GFP and examining whether Mei-p26 was present in Wh-GFP complex. Our results clearly showed that Wh interacts with Mei-p26 in the ovary (Fig. 4G).

The Wh-Mei-p26 interaction is evolutionarily conserved

As both Wh and Mei-p26 are highly conserved, we suspected that the Wh-Mei-p26 complex may be observable in other species. We thus expressed human orthologs of Wh tagged with Myc (WDR4-Myc) and Mei-p26 tagged with Flag (TRIM32-Flag) in human embryonic kidney 293T cells, a cell line often used for studying protein interactions. As expected, after pulling down Flag, WDR4-Myc was present in the TRIM-Flag complex (Fig. 4H), indicating an interaction between human WDR4 and TRIM32. To test whether human WDR4 can also function in *Drosophila* germ cells, we overexpressed *WDR4* in *wh* mutant germ cells using the *UAS-GAL4* system. Compared with 7-day-old wild-type ovaries bearing mature eggs with two dorsal appendages (as indicated by asterisks) (Fig. 4I, *n*=10), *wh*^{7} mutant ovaries were extremely small and rarely carried mature eggs (Fig. 4J, *n*=10). Overexpression of *WDR4* in the germline of *wh*^{7} mutant ovaries largely rescued ovary size, but not the number of mature eggs (Fig. 4K, *n*=15). In addition, massive branched fusomes (Fig. 4L,M), GSC loss (Fig. 4N) and stem-cyst formation (Fig. 4N′) were significantly suppressed by the expression of *WDR4* in *wh* mutant germ cells. Further, overexpression of *WDR4* in germ cells also rescued Orb enrichment in the oocyte of *wh*^{7} mutant egg chambers (Fig. 4O,P). Most importantly, sterility of *wh*^{7} mutants showed a trend toward rescue, although the difference did not reach statistical significance (*P*=0.06) (Fig. 4Q and wild-type egg production in Fig. 1C). This mild rescue phenotype could be due to a requirement for Wh in ovarian somatic cells or only partial functional replacement of Wh by WDR4. Nevertheless, our results suggest that the interaction between WD40 protein, Wh, and TRIM-NHL protein,

Development (2020) 147, dev182063. doi:10.1242/dev.182063

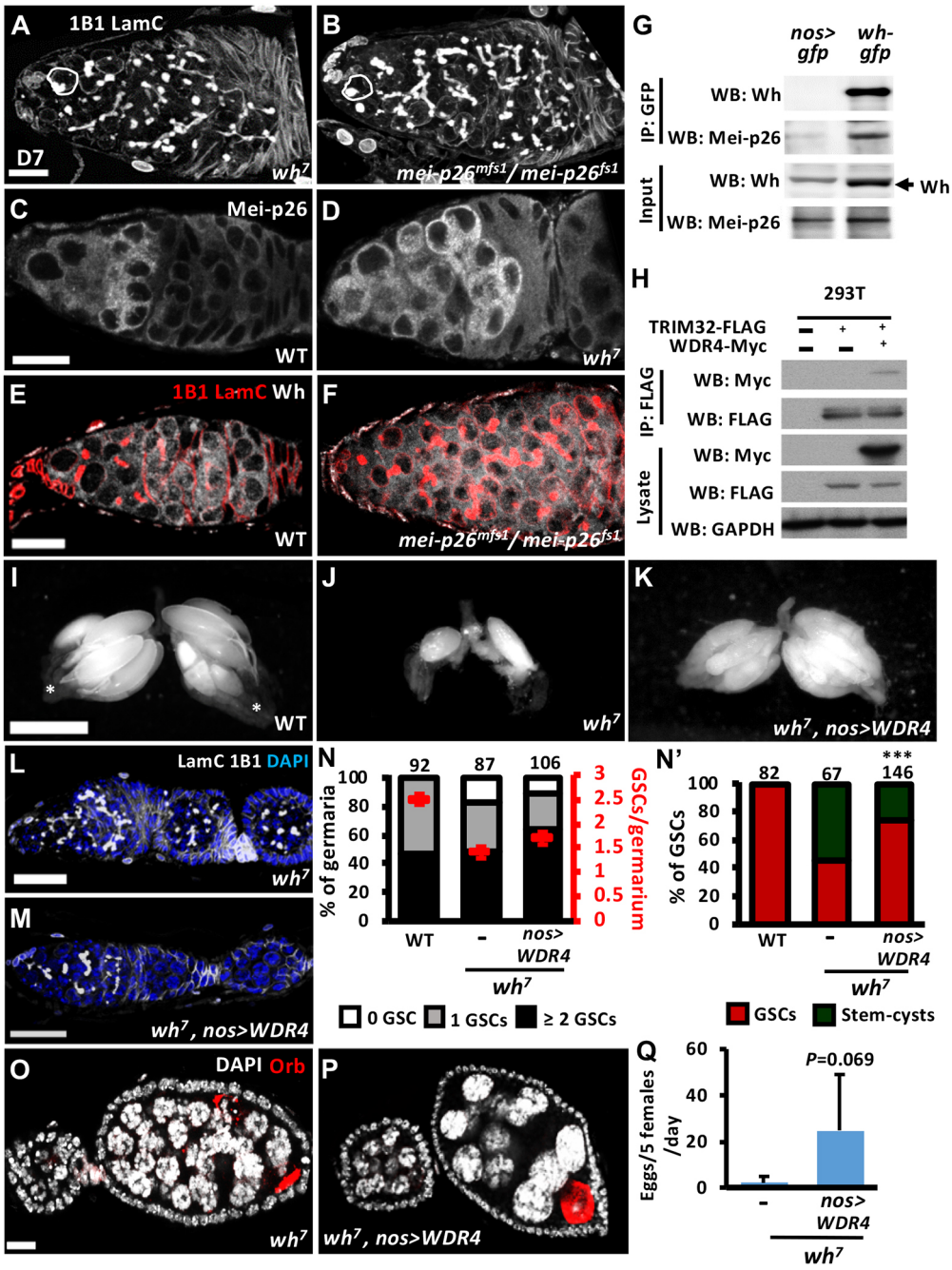

Fig. 4. Wh and Mei-p26 interaction is conserved and maintains germ cell homeostasis. (A,B) wh^7 (A) and $mei\text{-}p26^{mfs1}/mei\text{-}p26^{fs1}$ (B) mutant germaria showing 1B1 (gray, fusomes) and LamC (gray, terminal filament and cap cell nuclear envelopes). White solid lines outline GSCs. (C,D) Wild-type (C) and wh^7 mutant (D) germaria with Mei-p26 (gray). (E,F) Wild-type (E) and $mei\text{-}p26^{mfs1}/mei\text{-}p26^{fs1}$ mutant (F) germaria showing 1B1 (red), LamC (red) and Wh (gray). (G) Wh immunoprecipitates (IP) with Mei-P26 in the ovaries bearing *wh-gfp*. WB, western blotting using antibodies against indicated proteins. *nos>gfp* ovaries were used as a negative control for immunoprecipitation. Arrow shows Wh. (H) WDR4 immunoprecipitates with TRIM-32 in human 293T cells. Cells expressing the CMV empty vector, CMV-TRIM32-FLAG, or CMV-FLAG-TRIM32 plus CMV-WDR4-Myc were lysed and immunoprecipitated using anti-FLAG antibody, and 10% of lysate and immunoprecipitated protein complex were subjected for western blotting analysis using indicated antibodies. GAPDH was used as a loading control. (I-K) WT (I), wh^7 mutant (J) and wh^7, *nos>WDR4* mutant (K) germaria with a pair of one-week-old ovaries connected by the oviduct. Asterisks mark mature eggs. (L,M) wh^7 (L) and wh^7, *nos>WDR4* mutant (M) germaria showing 1B1 (gray), LamC (gray) and DAPI (blue). (N) Percentage of germaria with indicated GSC numbers in flies with indicated genotypes. Red *y*-axis (right) shows the average number of GSCs per germarium. Average values are indicated by red lines; data are mean±s.e.m. (N′) Percentage of normal GSCs or GSCs in stem-cysts in the germaria of indicated genotypes. Numbers of analyzed germaria are shown above each bar. (O-P) wh^7 (O) and wh^7, *nos>WDR4* mutant (P) egg chambers showing DAPI (gray) and Orb (red). (Q) The average number of eggs laid per female per day is shown; data are mean±s.d. Egg numbers were compared using two-tailed Student's *t*-test. Numbers of GSCs (N) and GSCs/stem-cysts (N′) were compared using a chi-squared test. Representative 7-day-old germaria are shown in 3D-reconstructed images. ***P<0.001. Genotype of wild-type is w^{1118}. Scale bars: 10 µm in A-F,L,M,O,P; 50 µm in I-K.

Development (2020) 147, dev182063. doi:10.1242/dev.182063

Table 1. *wh* and *mei-p26* mutants are highly similar at both phenotypic and molecular levels

Phenotype	Genotype	
	wh^{7}* or wh^{CRISPR}	*mei-p26*$^{mfs1/fs1}$‡
Female sterility	x	x‡
Stem-cyst formation	x	x
Highly branched fusome	x	x
Increased Brat expression	x	x
Attenuated Dpp signaling	x	x
GSC loss	x	x
Mitosis exit failure	x	M
Meiosis failure	x	x
Egg chamber carrying more or fewer than 16 germ cells	x	x
Overlapping expression of Bam and Nos	x	x
Increased ribosomal biogenesis	x	x
Elevated microRNA levels	x	x

*Molecular analyses of *wh* mutants were mainly performed on homozygous wh^{7} mutant females.

‡*mei-p26* mutants were analyzed previously (Li et al., 2012; Neumüller et al., 2008; Page et al., 2000; Sekelsky et al., 1999).

x, the indicated phenotype was observed in the mutant; M, the indicated phenotypes may be present in the mutant.

Note that highly branched fusomes are present in the entire *mei-p26* mutant germarium, as well as increased ribosomal biogenesis in *mei-p26* mutants, suggesting that *mei-p26* mutant germ cells also persist in mitosis.

Mei-p26, is evolutionarily conserved, and the interaction may be crucial for germ cell function in other organisms.

Wh in GSCs promotes Mei-p26-mediated BMP signaling to maintain GSCs

Mei-p26 is known to control GSC self-renewal via BMP signaling (Li et al., 2012). Upon GSC receipt of ligands from niche cap cells, BMP stemness signaling is activated, causing the phosphorylation of Mad (pMad) (Song et al., 2004), which suppresses transcription of the differentiation factor *bag of marbles* (*bam*) (McKearin and Ohlstein, 1995) (Fig. 5A). Expression of Mad is negatively regulated by Brat, and translation of Brat is suppressed by a Mei-p26 interaction with Nos (Fig. 5A) (Li et al., 2012). To test whether Wh affects Mei-p26-facilitated BMP signaling, we first examined expression of pMad and Brat. In wh^{7} mutant germaria, GSCs expressed similar levels of pMad compared with controls (Fig. 5B,D); however, expression of pMad was remarkably low in GSCs of stem-cysts (Fig. 5C,D). Compared with wild-type germaria (Fig. 5E), wh^{7} mutant germaria exhibited a dramatically increased Brat signal in germ cells (Fig. 5F) and ovary extracts (Fig. S5). Interestingly, Wh interacted with Nos in the ovary (Fig. 5G), suggesting that Wh might work in the same complex with Mei-p26 and Nos to silence *brat* translation. We proceeded to examine *bam* transcription using a *bamP: bam-gfp* transgene, which encodes a Bam-GFP fusion protein driven by the *bam* promoter (Chen and McKearin, 2003). Consistent with a previous report (Chen and McKearin, 2003), Bam-GFP was absent from GSCs and expressed in differentiated dividing germ cell cysts (2-8 cell cysts) in the control germarium (Fig. 5H). On the other hand, all germ cells within the wh^{7} stem-cyst expressed Bam-GFP (Fig. 5I), suggesting that these cells may be only partially differentiated. This result was confirmed by *in situ* hybridization to directly detect *bam* RNA distribution (Fig. 5J,K), although fusomes could not be clearly labeled in RNA-hybridized germaria. Thus, the upregulation of Bam expression in wh^{7} mutant GSCs of stem-cysts indicates that BMP signaling was disrupted in these cells.

To test whether upregulated Brat and Bam account for GSC loss in *wh* mutants, we attempted to reduce expression of Brat in wh^{7} flies. However, we failed to obtain adult wh^{7} mutant flies bearing either a copy of the *brat* null or hypomorphic allele, suggesting that Wh and Brat may play a crucial role during development. We then introduced a copy of the *bam* null allele (bam^{1}) and a *vasa-gfp* transgene to mark germ cells in wh^{7} homozygous mutants (Kai et al., 2005). Compared with controls (Fig. 5J), flies with *bam* reduced by one copy did not show rescued abnormal fusome morphology in differentiated cysts and distribution in the germarium (Fig. 5L), nor did reduction of *bam* rescue oocyte formation (Fig. 5M). However, removal of one copy of *bam* from wh^{7} mutant females completely restored GSC number (Fig. 5N; Fig. 2G). In addition, the number of wh^{7} mutants with stem-cysts was also significantly reduced (Fig. 5N′). These results indicate that upregulation of Bam in *wh* mutant germ cells is required for formation of stem-cysts, which precedes GSC loss.

Wh suppresses Nos translation, ribosomal biogenesis and microRNA levels in differentiated cysts

In differentiated cysts, Mei-p26 participates in the differentiation program via multiple regulatory actions (Fig. 6A). First, Mei-p26 forms a complex with Bgcn, Sxl and Bam to silence the translation of Nos (Li et al., 2013); *nos* deletion has been shown to cause GSC loss (Wang and Lin, 2004). Second, Mei-p26 represses ribosomal biogenesis (promoting cell proliferation; Donati et al., 2012) by suppressing expression of dMyc (also known as Myc) (McKearin, 1997), a master regulator of ribosomal biogenesis (van Riggelen et al., 2010). Third, Mei-p26 inhibits expression of a subset of microRNAs that are involved in differentiation (Neumüller et al., 2008), via an unknown mechanism. To understand the extent to which Wh works with Mei-p26 in differentiated germ cells, we examined whether Wh deficiency affects the known molecular functions of Mei-p26.

To test whether Wh promotes differentiation by the same mechanism as Mei-p26, we first examined microRNA levels in *wh* and *mei-p26* mutant ovaries by microRNA-seq analysis. Indeed, expression of the same subset of microRNAs was increased in wh^{7} mutant ovaries (Fig. 6B) and *mei-p26*^{mfs1}/*mei-p26*^{fs1} mutant ovaries (Fig. 6B); this subset also agreed with a previous report (Neumüller et al., 2008). We validated this result with qRT-PCR for three microRNAs, *mir-1*, *mir-289*, and *mir-316* (Fig. 6C). These results suggest that Wh may interact with Mei-p26 to suppress expression of several microRNAs. We also examined Nos expression in *wh* mutant germaria. In the control germarium (Fig. 6D; Table S2), Bam (*bamP: bam-gfp*) and Nos were expressed in different cysts. However, Bam and Nos were co-expressed in wh^{7} mutant germ cells (Fig. 6E), suggesting that translational silencing of Nos by Bam is dependent on the presence of Wh. To test this hypothesis, we examined whether Wh is required for the Bam-Sxl-Bgcn-Mei-p26 complex to target the 3′ untranslated region (UTR) of *nos* mRNA using RNA-immunoprecipitation followed by RT-PCR. As previously reported (Li et al., 2013), we found that *nos* mRNA could be immunoprecipitated with Sxl antibody but not IgG in wild-type ovary lysate, but this immunoprecipitation did not occur in wh^{7} mutant ovary lysate (Fig. 6F). In addition, a pull-down assay using ovary extracts revealed that Wh weakly interacted with Bgcn (Fig. 6G); however, we failed to pull down Bam and Sxl (data not shown), possibly owing to a weak interaction between the proteins or because Wh only promotes Mei-p26 inclusion in the Bgcn-Bam-Sxl complex. This result suggests that the overlapping expression of Nos and Bam in wh^{7} mutant germ cells occurs

Development (2020) 147, dev182063. doi:10.1242/dev.182063

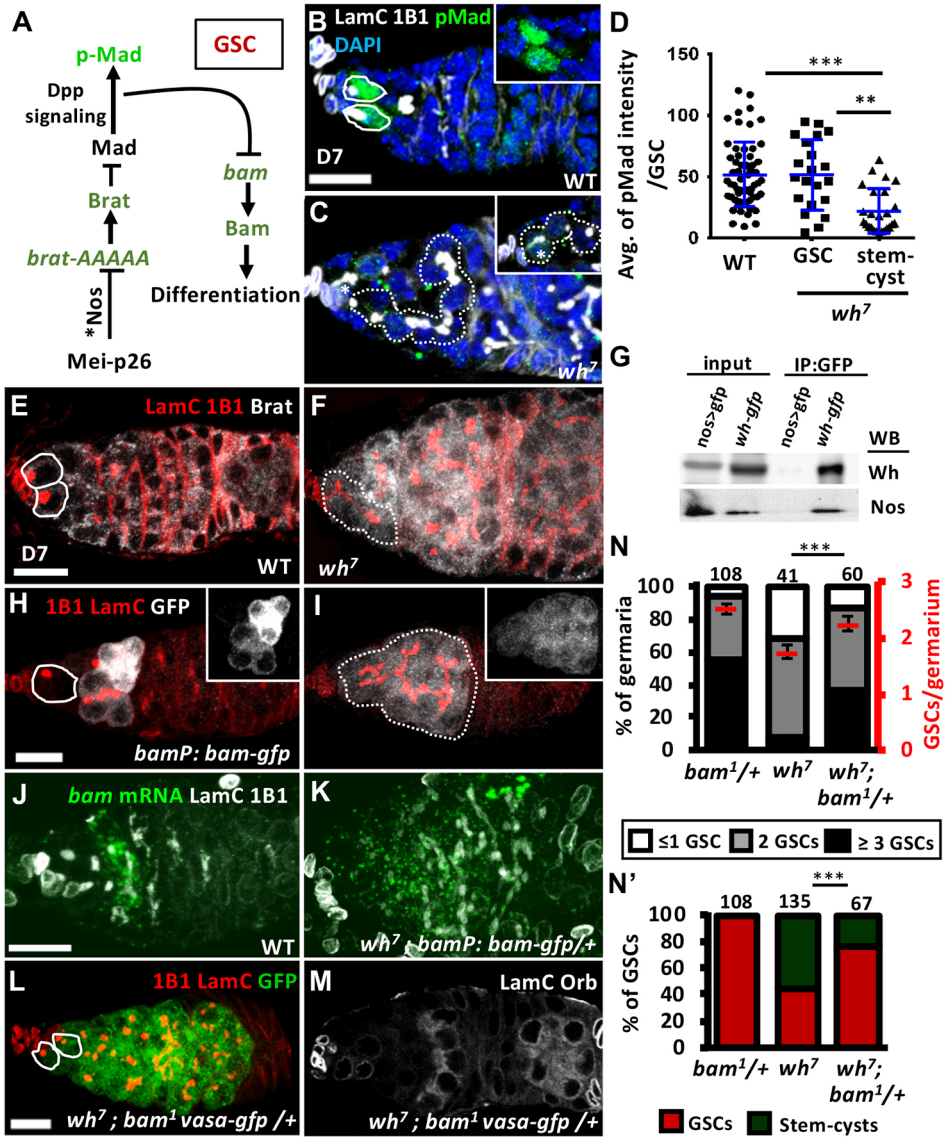

Fig. 5. Wh promotes Dpp-mediated Bam silencing in GSCs. (A) The known role of Mei-p26 in GSC maintenance. In the wild-type GSC, Mei-p26 and Nos form a complex to inhibit Brat translation, allowing Mad to be stabilized and phosphorylated by BMP signaling. Phosphorylated Mad (pMad) translocates into the nucleus to suppress *bam* transcription. Asterisk indicates the interaction with Mei-p26. (B,C) Wild-type (WT) (B) and wh^7 mutant (C) germaria showing 1B1 (gray, fusomes), LamC (gray, terminal filament and cap cell nuclear envelopes), pMad (green, BMP signaling) and DAPI (blue, DNA) labeling. The inset in B shows pMad in GSC with DAPI and pMad channels only. The inset in C shows another stem-cyst marked by the asterisk from a different focal plane. (D) Average intensity of pMad in control GSCs, or in GSCs within stem-cysts of flies with indicated genotype; data are mean±s.d. (E,F) Wild-type (E) and wh^7 mutant (F) germaria showing 1B1 (red), LamC (red) and Brat (gray). (G) Wh immunoprecipitates (IP) with Nos in the ovaries bearing wh-gfp. WB, western blotting using antibodies against indicated proteins. *nos>gfp* ovaries were used as a negative control for immunoprecipitation. (H,I) Control (H) and wh^7 mutant (I) germaria with two copies or one copy of *bamP: bam-gfp* (gray, *bam* transcription reporter), respectively, showing 1B1 (red) and LamC (red) labeling. Insets show only GFP channel. (J,K) *In situ* hybridized wild-type (J) and wh^7 mutant (K) germaria showing 1B1 (gray), LamC (gray) and *bam* mRNA (green). (L,M) wh^7 mutant germaria bearing a bam^1 mutant allele and a *vasa-gfp* transgene (green, germ cells) showing 1B1 (red) and LamC (red) (L), and LamC (gray) and Orb (gray, oocyte marker) (M). (N) Percentage of germaria with indicated GSC numbers in flies with indicated genotypes. Red *y*-axis (right) shows the average number of GSCs per germarium. Average values are indicated by red lines; error bars represent s.e.m. (N′) Percentage of normal GSCs or GSCs in stem-cysts in the germaria of indicated genotypes. Numbers of GSCs (N) and GSCs/stem-cysts (N′) were compared using a chi-squared test. Numbers of analyzed germaria are shown above each bar. Solid lines mark GSCs; dotted lines circle stem-cysts. Representative 7-day-old germaria are shown in 3D reconstructive images. Genotype of wild-type is w^{1118}. **P<0.01; ***P<0.001. Scale bars: 10 µm.

because, in the absence of Wh, the Mei-p26-Bgcn-Bam-Sxl complex is not functional or not formed.

We also examined ribosomal biogenesis by labeling Fibrillarin to mark nucleoli (Fomproix et al., 1998). Ribosomal biogenesis takes place within nucleoli, and bigger nucleolar size represents higher ribosomal biogenesis activity (Grewal et al., 2005; Rudra and Warner, 2004). In the wild-type germarium (n=12) (Fig. 6H), the sizes of nucleoli (0.7±0.05 µm^2) in GSCs and early germ cells were larger than those in differentiated cysts (0.4±0.02 µm^2, P<0.001), consistent with a previous report that showed ribosomal biogenesis is negatively correlated with differentiation status (Neumüller et al., 2008). In contrast, in wh^7 mutant germaria and *nos>wh*^{RNAi} germaria (Fig. 6I,L), nucleoli in germ cells had larger or comparable sizes with those in wild-type GSCs or early germ

Development (2020) 147, dev182063. doi:10.1242/dev.182063

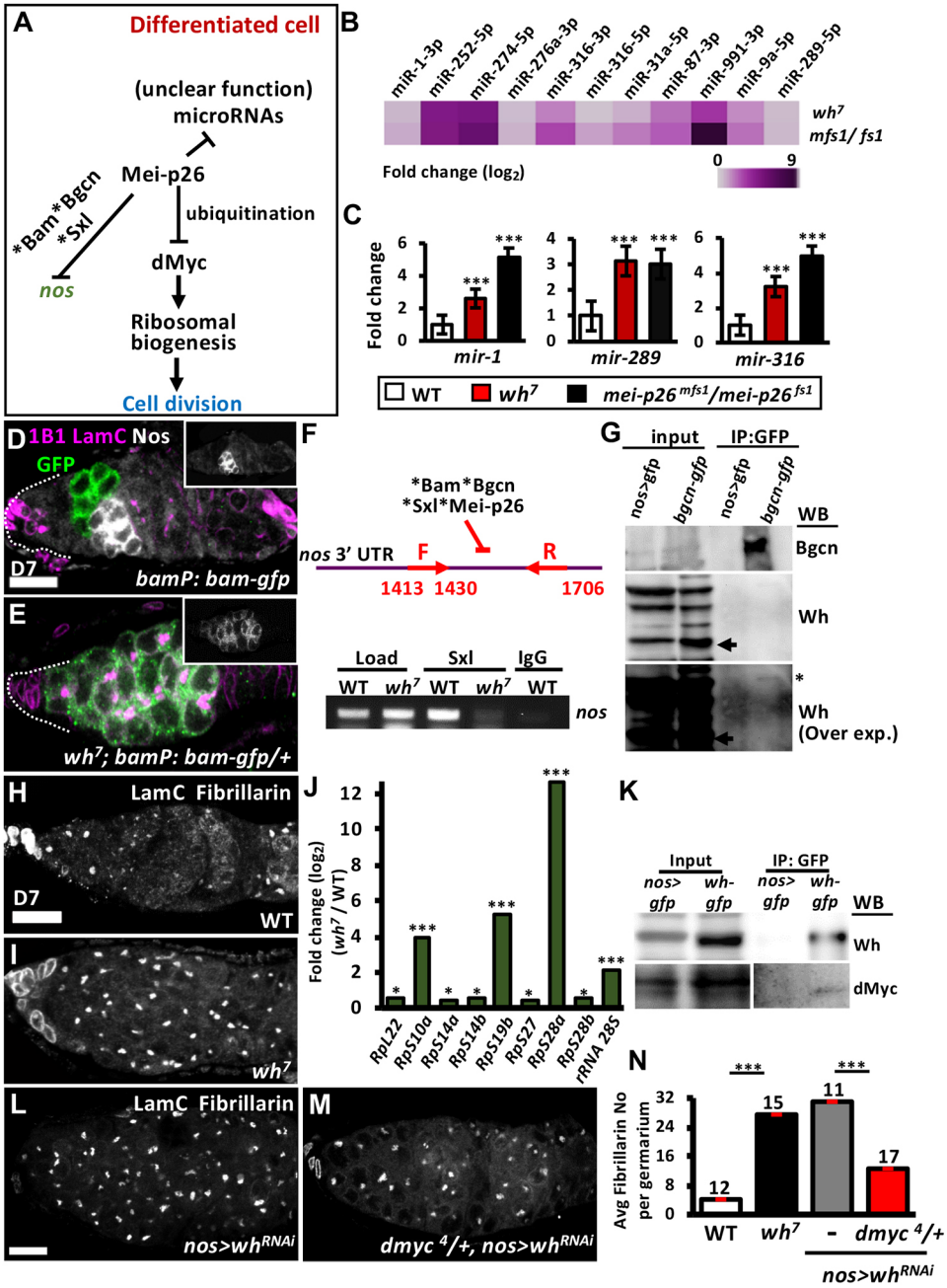

Fig. 6. Wh is required for Mei-p26 function for germ cell differentiation. (A) The known role of Mei-p26 in differentiating germ cells. In the wild-type cystoblast or differentiated cyst, Mei-p26 promotes differentiation via multiple mechanisms. Mei-p26 forms a complex with Bam, Sxl and Bgcn to suppress *nos* translation. Mei-p26 also reduces microRNA levels via unknown mechanisms, and it causes degradation of dMyc to reduce ribosomal biogenesis. Asterisks indicate the interaction with Mei-p26. (B) Heat maps show $\log_2$ fold changes of significantly upregulated microRNAs in *wh*^{7} and *mei-p26*^{mfs1}/*mei-p26*^{fs1} mutant ovaries. Color gradient represents fold change of the indicated microRNA. (C) qRT-PCR expression analysis of indicated microRNAs; data are mean±s.d. (D,E) Control (D) and *wh*^{7} mutant (E) germaria bearing two copies and one copy of *bamP: bam-gfp*, respectively, showing 1B1 (magenta), LamC (magenta), GFP (green) and Nos (gray) labeling. Dotted lines mark the anterior edge of the germarium. Insets show Nos channel only. (F) In the absence of Wh, the Mei-p26-Bgcn-Bam-Sxl complex fails to target to *nos* mRNA. Immunoprecipitation of Sxl but not IgG enriches *nos* 3′ UTR amplified from the region targeted by the Sxl-Bam-Bgcn-Mei-p26 complex, using forward (F, 1413-1430 bp of the *nos* transcripts) and reverse (R, 1706-1695bp) primers. Total RNA from wild-type and *wh*^{7} mutant ovaries used as templates for *nos* amplification served as a loading control. (G) Bgcn immunoprecipitates Wh in ovaries bearing *bgcn-gfp*. Arrows indicate endogenous Wh; asterisk marks Wh after IP. WB, western blotting using GFP and Wh against indicated proteins. (H,I) Wild-type (H) and *wh*^{7} mutant (I) germaria showing LamC (gray) and Fibrillarin (gray, nucleoli). (J) RNA-seq results showing ribosomal gene transcripts are increased in 7-day-old *wh*^{7} mutant ovaries compared with wild-type controls. (K) Wh immunoprecipitates (IP) dMyc in ovaries bearing *wh-gfp*. WB, western blotting using antibodies against indicated proteins. (L,M) Control (*nos>wh*^{RNAi}) (L) and *dmyc*^{4}/+, *nos>wh*^{RNAi} (M) germaria showing LamC (gray) and Fibrillarin (gray, nucleoli). (N) Average number of nucleoli marked with Fibrillarin that are present in GSCs and early germ cells in the germarium of indicated genotypes; data are mean±s.e.m. the number of analyzed germaria are shown above each bar. The fold changes in C, J and average Fibrillarin in N were compared using two-tailed Student's *t*-test. *nos>gfp* ovaries were used as a negative control for immunoprecipitations in G and K; over exp., over exposure in G. **P*<0.05; ****P*<0.001. Representative 7-day-old germaria are shown in 3D-reconstructed images. The genotype of wild-type is *w*^{1118}. Scale bars: 10 µm.

Development (2020) 147, dev182063. doi:10.1242/dev.182063

cells, and large nucleoli were distributed throughout the germarium. RNA-seq analysis also showed that several ribosomal genes were upregulated (Fig. 6J). Interestingly, immunoprecipitation with ovary lysates showed that Wh interacted with dMyc (Fig. 6K), which is targeted by Mei-p26 for degradation in the wing disc (Ferreira et al., 2014). Removal of one *dmyc* copy from *nos>wh*^{RNAi} germaria significantly rescued the number of large nucleoli present in GSCs or early germ cells (Fig. 6L-N). In addition to the reduction in number of large nucleoli, massive branched fusomes and germ cell number (revealed by smaller germarial size) was also partially rescued; however, meiosis was still impaired (Fig. S6). These results suggested that Wh controls germ cell mitosis at least in part via ribosomal biogenesis. Taken together, our results show that Wh and Mei-p26 work in the same complex, and the function of Mei-p26 to maintain germline homeostasis relies on Wh.

DISCUSSION

Wh regulates stem cell self-renewal and differentiation via Mei-p26

Homeostatic regulation of stem cells (Hannezo et al., 2014; Jörg et al., 2019 preprint), the very foundation of tissue homeostasis, remains poorly understood at a molecular level. Using the *Drosophila* GSC lineage as an *in vivo* model to study stem cell biology, we found that Wh, a WD40 protein, controls GSC self-renewal and differentiation via Mei-p26, a TRIM-NHL protein (Fig. 7). An interaction between the proteins was identified in the ovary, and striking similarities between *wh*^{7} and *mei-p26* mutants were observed at both phenotypic and molecular levels (Table 1). Based on our findings and published results regarding Mei-p26 function, we propose that, in wild-type GSCs, Wh, Mei-p26 and Nos form a complex to inhibit *brat* translation, allowing Mad to be stabilized and phosphorylated by BMP signaling. pMad then translocates to the nucleus, where it suppresses transcription of *bam*, a master regulator of differentiation. On the other hand, Wh also promotes differentiation of GSC progeny by multiple mechanisms. First, Wh, Mei-p26, Bgcn, Sxl and Bam form a complex that binds to the 3′ UTR of *nos* to silence its translation, possibly helping to turn off BMP signaling in the differentiating GSC progeny. Second, Wh interacts with Mei-p26, an E3 ubquitin ligase, to control dMyc protein levels and allow proper ribosomal biogenesis. Third, the interaction between Wh and Mei-p26 also limits expression of a subset of microRNA, which may contribute to differentiation. These functions of Wh appear to be especially important for the last step of cytokinesis (abscission), which is completed between the GSC and its daughter cell after early G2 phase, as revealed by closure of the ring canal.

In *wh* mutant GSCs, *brat* translation is not suppressed, decreasing the level of pMad and increasing the expression of the differentiation factor Bam. This sequence of events causes premature differentiation of GSCs and leads to GSC loss,

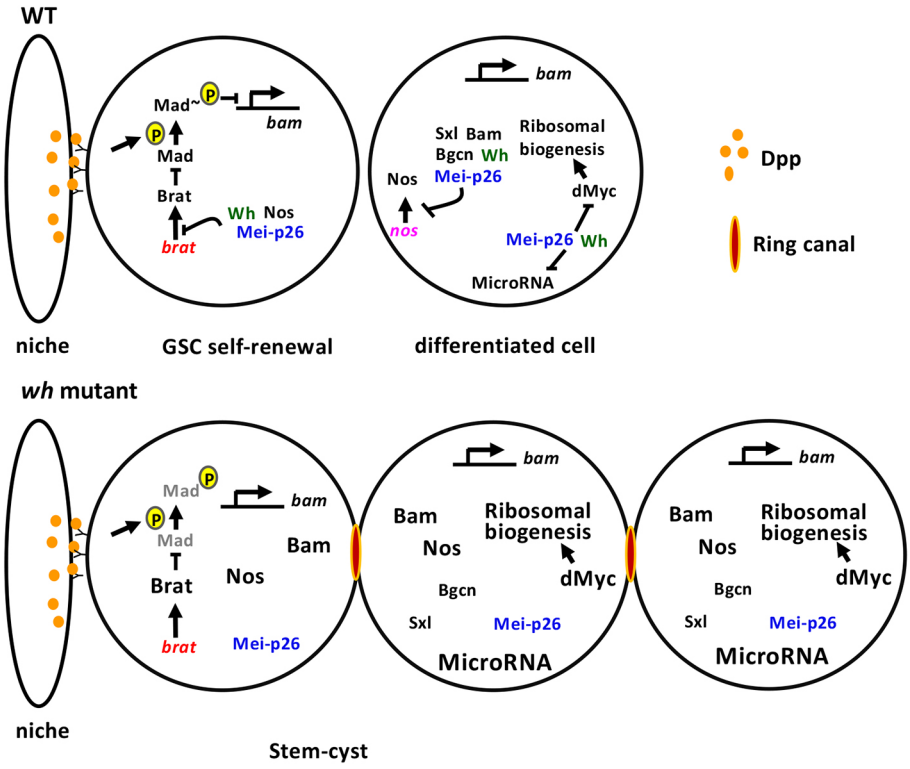

Fig. 7. Model of Wh coordination with Mei-p26 to control the balance between GSC self-renewal and differentiation. In wild-type (WT) GSCs, Wh interacts with Mei-p26 and Nos to suppress *brat* translation, allowing maintained Mad expression to turn on BMP signaling and repress *bam* transcription, thus promoting GSC self-renewal. In the cystoblast (CB) or the differentiated germ cell, Wh interacts with Mei-p26 in a different complex to facilitate differentiation and transition from mitosis to meiosis. The Wh-Mei-p26-Sxl-Bam-Bgcn protein complex suppresses *nos* translation, whereas Wh-Mei-p26 also targets dMyC for degradation, thereby suppressing ribosomal biogenesis. Moreover, Wh-Mei-p26 limits microRNA expression. In the absence of Wh, Mei-p26 is dysfunctional in the GSC lineage. In GSCs, Brat is upregulated to reduce Mad expression, resulting in elevated expression of Bam and precocious differentiation of GSCs, forming a stem-cyst, in which GSCs are interconnected with more than one daughter through open ring canals. In the CB or differentiated germ cell, Mei-p26 cannot repress *nos* translation which results in overlapping expression of Bam and Nos. MicroRNA levels are elevated. Moreover, Mei-p26 does not function to degrade dMyc, which drives excessive ribosomal biogenesis and cell division. These actions lead to overproliferation, mitotic persistence and meiotic failure in germ cells, causing sterility.

Development (2020) 147, dev182063. doi:10.1242/dev.182063

consistent with the known roles of Brat and Bam in germ cell differentiation. Mutation of *brat* or *bam* increases GSC number, whereas overexpression of *brat* or *bam* in germ cells causes germ cell depletion by forcing GSC differentiation (Harris et al., 2011; McKearin and Ohlstein, 1995; Ohlstein and McKearin, 1997). Mutation of *wh* in germ cells also results in incomplete abscission between GSCs and daughter cells, leaving open ring canals that create stem-cysts. Although we did not determine the molecular mechanism by which Wh controls GSC abscission, removing a copy of *bam* significantly reduced stem-cyst number in *wh* mutant germaria, which suggests a role for Bam in Wh control of GSC abscission. In *wh* mutant germaria, stem-cysts simultaneously express Nos (a GSC maintenance factor) and Bam; thus, the growths display characteristics of both GSCs and daughter cells. In addition, ribosomal biogenesis is promoted via upregulated dMyc and drives germ cell overproliferation. Lastly, some differentiation-associated microRNAs are increased in the mutant ovaries, although their functions are not yet clear. We do not know whether a defect in meiosis is a consequence of overproliferative *wh* mutant germ cells, or whether Wh has a separate role in meiosis.

Our results show that Wh is required for Mei-p26 function in germ cell homeostasis. However, it is unclear whether Wh directly interacts with Mei-p26 and which domains in the two proteins mediate the interaction. It is possible that Wh serves as a bridge for Mei-p26 to interact with its known partners. We observed an interaction between human orthologs of Wh (WDR4) and Mei-p26 (TRIM32), suggesting that the interaction is evolutionarily conserved. Thus, the interaction between WD40 and TRIM-NHL proteins may be crucial for stem cell regulation in other organisms.

Wh depletion delays GSC abscission at least partly via effects on Bam

The last step in cell division, cytokinesis, is completed by abscission, which physically separates the two daughter cells. Cytokinesis starts by ingression of the cleavage furrow, constricting the plasma membrane onto the spindle midzone to form an electron-dense structure, the midbody, which comprises a thin membrane channel bridging two nascent daughter cells (Nähse et al., 2017). The stem-cyst forms owing to a failure of GSCs to separate from daughter cells. Two possible mechanisms may produce such an abscission failure. First, a stem-cell-specific defect may prevent GSC-CB abscission. Second, GSCs may exhibit characteristics of differentiating cells that cause them to adopt incomplete cell cytokinesis programs. In addition to controlling chromosome orientation and segmentation, Aurora B is known to intrinsically regulate the timing of cell abscission (Nähse et al., 2017), including in *Drosophila* female GSCs (Mathieu et al., 2013). During abscission, Aurora B in GSCs is targeted to the midbody and triggers membrane abscission via Endosomal sorting complex required for transport III (ESCRT-III) machinery (Eikenes et al., 2015; Matias et al., 2015; Nähse et al., 2017). Aurora B negatively controls ESCRT-III, i.e. when Aurora B is active, ESCRT-III activity is low and abscission is delayed, and vice versa. It has also been shown that ribosomal biogenesis coordinates with ESCRT-III in GSCs to promote GSC abscission (Sanchez et al., 2016). Increasing Aurora B activity or disrupting ESCRT-III generates stem-cysts with germ cells that undergo synchronous division, yielding 32 germ cells in most egg chambers (Eikenes et al., 2015; Mathieu et al., 2013; Matias et al., 2015). However, *wh* mutant germ cells within stem-cysts divide asynchronously with elevated ribosomal biogenesis, and *wh* mutant egg chambers carry various numbers of germ cells. In addition, in *wh* mutant stem-cysts, decreased pMad expression, upregulated Bam expression and branched fusomes are all hallmarks of differentiating cysts. These results suggest that *wh* mutant stem-cysts may adopt the abscission program of differentiating cysts. Interestingly, removing a copy of *bam* from *wh* mutants or from *shrub* (a subunit of ESCRT-III) mutants partially rescues stem-cysts (Sanchez et al., 2016), suggesting that GSC abscission is coupled with cell fate. Further studies will be required to understand the molecular targets of Wh that control GSC abscission, and how GSCs and differentiating cysts acquire different abscission programs. Nevertheless, our study has shown that Wh participates with Mei-p26 to regulate fate determination in stem cells and daughter cells. This novel interaction may be conserved in other species and introduces the idea that WD40 proteins may participate with TRIM-NHL proteins in cell fate decision.

MATERIALS AND METHODS

Drosophila strains and cultures

Drosophila stocks were maintained at 22-25°C on standard medium. w^{1118} was used as a wild-type control. Null wh^{7}, bam^{1} (a gift from A. Spradling, Carnegie Institution for Science, Washington, DC, USA), $mei\text{-}p26^{mfs1}$ [Bloomington *Drosophila* Stock Center (BDSC), BL5919], $brat^{11}$ (a gift from C.Y. Lee, University of Michigan, USA), $dmyc^{4}$ (BDSC, BL64769), hypomorphic $mei\text{-}p26^{fs1}$ (a gift from P. Lasko, McGill University, Quebec, Canada) and $brat^{Df}$ alleles (a gift from C.Y. Lee) have been described (Arama et al., 2000; Hsu et al., 2008; Page et al., 2000; Pierce et al., 2004). wh^{CRISPR} is a genetic null allele generated by the CRISPR/Cas9 system (WellGenetics, Taipei, Taiwan). *p53R-gfp* (nls) (a gift from J.M. Abrams, University of Texas Southwestern Medical Center, USA) is a p53 sensor containing a well-characterized conserved p53 binding site placed upstream of a nucleus-targeted GFP (Wylie et al., 2014). *bamP: bam-gfp* contains a *bam-gfp* coding sequence driven by the *bam* promoter (Chen and McKearin, 2003), and *bgcnP: bgcn-gfp* (a gift from M. Buszczak, University of Texas Southwestern Medical Center, USA) is a *bgcn-gfp* coding sequence driven by the *bgcn* promoter (Li et al., 2009). *p[wh-gfp]* is a genomic control bearing the *wh* gene with in-frame fusion of *gfp* to its C terminus (Wu et al., 2006). *dmyc-gfp* (BDSC, BL38633) was used to monitor dMyc expression, although we found that dMyc-GFP did not mimic the dMyc expression pattern, which was highly expressed in GSCs and early germ cells, but decreased in 16-cell cysts (Neumüller et al., 2008). Efficiency of the *UAS-RNAi* lines against *wh* (BDSC, BL61281) was tested (Fig. 2J,K). The *nanos-GAL4-VP16* was used to express transgene in the germline (Rørth, 1998). Flies expressing *RNAi* were cultured throughout development at 29°C to allow for GAL4 expression. For the egg laying assay, newly eclosed females were cultured with w^{1118} males for 1 day at 25°C, then transferred into plastic bottles capped with 35 mm molasses petri dishes supplied with a layer of wet yeast (replaced daily). Small holes were drilled in the bottom of the bottle to allow air flow. To measure egg production, five pairs of flies per bottle, which were placed upside down, were cultured for a period of 4-5 days and the number of eggs on the molasses petri dishes was counted every 24 h in triplicate. Other genetic elements are described in FlyBase (http://flybase.org).

Genetic mosaic analysis

Genetic mosaic clones were generated by FLP/FRT-mediated mitotic recombination (Xu and Rubin, 1993). Flies of genotypes $hs\text{-}flp^{122}$ *ubi-gfpFRT19A/FRT19A*, $hs\text{-}flp^{122}$*ubi-gfpFRT19A/*wh^{7}*FRT19A* and $hs\text{-}flp^{122}$*ubi-gfpFRT19A/*wh^{CRISPR}*FRT19A* were generated from standard crosses. The newly eclosed females with genotypes described above were fed on yeast diets for 1 day at 25°C, then subjected to heat shock for 1 h at 37°C twice daily at 10-12 h intervals for three days. After heat shock, flies were cultured at 25°C until dissection; food with dry yeast was changed daily. Homozygous mutant cells were identified by the absence of GFP.

Transgenic fly generation

A full length of human WDR4 was amplified from *pRK5M-WDR4* (Wang et al., 2017) by PCR using a pair of primers carrying SpeI and BamHI sites

Development (2020) 147, dev182063. doi:10.1242/dev.182063

(primer sequences are listed in Table S1). The amplified fragment was digested with SpeI and BamHI and subcloned into the *pUASpattB* vector to create *pUASp-WDR4*. Transgenic lines were generated as described previously (Spradling and Rubin, 1982).

Immunofluorescence

Ovaries were dissected in Grace's insect medium (Lonza, 04-457F0) at room temperature (RT) within 15 min and fixed with 5% (w/v) paraformaldehyde (PFA; Alfa Aesar, 30525-89-4) for 13 min at RT, after which samples were washed and stained as previously described (Su et al., 2018). The following primary antibodies were used at the indicated dilutions in blocking buffer (Goal Bio, GBW-3400): mouse anti-1B1 [1:30, Developmental Studies Hybridoma Bank (DSHB), 7H9 1B1], mouse anti-LamC (1:40, DSHB, LC28.26), mouse anti-BrdU (1:20, BD Biosciences, clone B44), mouse anti-Fasciclin III (1:40, DSHB, 7G10), rabbit anti-Vasa (1:250, Santa Cruz Biotechnology, sc-30210), mouse anti-C(3)G (1:500, a gift from R.S. Hawley, Stowers Institute, USA), rabbit anti-Mei-p26 (1:500, gift from P. Lasko), rabbit anti-Cleaved caspase III (Asp175) (1/1000, Cell Signaling Technology, 9661), rabbit anti-gfp (1:1000, Torrey Pines Biolabs, TP401), rabbit anti-Histone H2AvD pS137 (1:1000, Rockland, 600-401-914), rabbit anti-Phospho-Histone H3 (Ser10) (1:250, Millipore, 06-570), rabbit anti-Brat (1:200, a gift from J. Noblich, IMBA, Austria), rabbit anti-Vasa (1:250, Santa Cruz Biotechnology, sc-30210), rabbit anti-Nos (1:1000, a gift from K.H. Nakamura, Kumamoto University, Japan), rabbit anti-*Drosophila* Wh (1:500, generated by T.-S. Hsieh at Duke University, USA), rabbit anti-phospho-Mad (1:200, a gift from E. Laufer, Columbia University, USA) and rabbit anti-dMyc (1:5000, a gift from D. Stein, The University of Texas at Austin, USA). Note, we did not observe expression patterns similar to those previously described, where dMyc expression is high in GSCs/early germ cells and decreased in 16-cell cysts (Neumüller et al., 2008). ApopTag® Fluorescein *In Situ* Apoptosis Detection Kit (Merck, S7110) was used as previously described (Hsu and Drummond-Barbosa, 2009). BrdU incorporation was performed as previously described (Hsu et al., 2008). Ovaries were incubated with primary antibodies at 4°C overnight (O/N), washed in PBS with 0.1% Triton X-100 (PBST) 3 times, each for 20 min, and then stained with secondary antibodies, as follows: Alexa Flour 488 anti-rabbit (1:500, Invitrogen, A1008), Alexa Flour 568 anti-mouse (1:250, Invitrogen, A11077), Alexa Flour 633 anti-rabbit (1:250, Invitrogen, A21070) and Alexa Flour 633 anti-mouse (1:250, Invitrogen, A21094). Samples were incubated in 0.5 µg/ml DAPI, mounted in mounting solution [2% N-propyl gallate (Sigma-Aldrich, P-3130), 85% glycerol] and analyzed using a Zeiss LSM 700 confocal microscope. *Z*-stack images were acquired from the anterior part of the ovary on a Zeiss LSM 700 confocal microscope with a 40× or 60× oil immersion lens using identical acquisition conditions for each individual experiment. The image analysis was performed as experimental replicates. At least twenty flies were randomly examined per experiment and 5-7 germaria per ovary were picked to increase the frequency in the population. The total number of examined germaria is indicated for each individual experiment.

GSCs were characterized by placement of the fusome (spectrosome, labeled by 1B1) adjacent to the cap cell niche (oval-shaped cells labeled by LamC). GSCs interconnected with more than one germ cell by round/branched-shaped fusomes were identified as stem-cysts, in which GSC abscission was not complete. To quantify pMad expression, ImageJ was used to calculate the average fluorescence intensity in confocal *z*-stacks at the largest peripheral of GSCs or stem-cysts. To quantify the size of nucleoli labeled by Fibrillarin, ImageJ was used to calculate the area. All data were recorded in Excel, and two-tailed Student's *t*-test or chi-squared test were used to evaluate statistically significant differences; **P*<0.05, ***P*<0.01, ****P*<0.001.

In situ hybridization

To generate *bam* probes for *in situ* hybridization, the coding region of *bam* (980 bp) was amplified from the ovary cDNA (described below), using primer pairs (Table S1), and subcloned into the pGEM-T-Easy vector (Promega). Antisense RNA probes labeled with digoxigenin (DIG)-UTP (Roche) were synthesized from 1 µg of pGEM-T-*bam* plasmids digested with NcoI using the ampliCap™ SP6 high-yield message marker kit (Cell Script). Fluorescent RNA *in situ* hybridization was performed as previously reported (Tseng et al., 2018), with slight modifications. In brief, ovaries were dissected in Grace insect medium (Lonza) and fixed using 4% PFA in PBS (DEPC-treated) with freshly added 1% DMSO for 20 min at RT or at 4°C overnight. Samples were washed in PBS and dehydrated in an ethanol series (diluted in PBS: 25%, 50%, 75% and 100%) and were stored at −20°C for least one night. Samples were then rehydrated through an ethanol series (100%, 75%, 50% and 25%), rinsed with PBS, treated with 50 µg/ml Proteinase K (in PBS; Sigma-Aldrich, 003115836001) for 5 min at RT. After post-fixing with 4% PFA in PBST (1× PBS with 0.1% Tween 20) for 30 min at RT, samples were washed in 1 ml PBT (0.1% Tween 20, 0.1% DEPC) twice for 15 min, and three times for 5 min and prehybridized in hybridization buffer (HYB^+) (50% formamide, 5× SSC, 50 µg/ml heparin, 0.1% Tween 20, 100 µg/ml tRNA, 10 µg/ml salmon sperm DNA) for 1 h at 60°C. Hybridization was performed in HYB^+ containing denatured DIG-labeled RNA probes (100-150 ng) at 60°C O/N. Samples were washed with a series of HYB^- (50% formamide, 5× SSC with 0.1% Tween 20) solutions in 2× SSC (0.3 M NaCl, 30 mM sodium citrate; 75%, 50% and 25%) at 65°C and a series of 0.2× SSC solutions (75%, 50% and 25%) at 68°C, followed by rinsing with PBST at RT. Samples were treated with 3% H_2O_2/PBT for 1 h at RT to inactivate endogenous perioxidase and then blocked in 2× Roche Blocking solution for 1 h at RT. Ovaries were incubated with anti-Dig-POD (1:500, Roche, 11207733910) in blocking buffer at 4°C overnight, washed well, and incubated in 1:200 TSA/amplification buffer (TSA Plus Fluorescence Kits, PerkinElmer) for 30 min to develop signals. After washing, ovaries were blocked with blocking solution (GOAL Bio) and then subjected to the immunostaining procedure.

Drosophila Wh protein purification for antibody generation

Recombinant Wh protein with a hexahistidine tag at the C terminus was produced and purified from Rosetta™(DE3) pLysS Competent Cells (Novagen, 70956-4CN) carrying the *wh*-expressing ET23b vector (Wu et al., 2006). In brief, Wh-His expression was induced in Rosetta cells by adding 1 mM IPTG for 4 h at 37°C. The cells were harvested and re-suspended in lysis buffer [100 mM NaCl, 10 mM Tris/HCl, 5 mM β-ME, 10% glycerol, protease inhibitor mixture (cOmplete Tablet, Mini EDTA-free, EASYpack, Roche)]. After sonication, the supernatant from the cell lysate was applied to equilibrated Ni Sepharose™ 6 Fast Flow beads (GE Healthcare). Wh-His protein-bound Ni beads were first washed with Tris buffer [300 mM NaCl, 10 mM Tris/HCl, 8 M urea (pH 5.9)] to remove low-affinity bound proteins. Next, Wh-His was eluted from the beads with a lower pH Tris buffer [300 mM NaCl, 10 mM Tris/HCl, 8 M urea (pH 4.5)]. The purified protein was used as an antigen to immunize rabbit (Abnova, Taiwan). As shown in Fig. 1E, Wh protein is absent in *wh* mutant nucleus and cytoplasmic fractions, demonstrating the specificity of the Wh antibody.

Subcellular fractionation

Ten or 40 pairs of ovaries from full grown or newly eclosed flies were homogenized in 100 µl EBI buffer [10 mM HEPES (pH 7.5), 1.5 mM $MgCl_2$, 10 mM KCl] plus 1% NP40 and protease inhibitor mixture (cOmplete™, Sigma-Aldrich). The homogenate was vortexed vigorously on ice for 5 min and centrifuged at 1700 ***g*** for 3 min at 4°C. The precipitant (nuclear pellet) was washed with 1 ml EBI plus 1% NP40 and protease inhibitors (cOmplete™, Sigma-Aldrich) by pipetting, and centrifuged at 1700 ***g*** for 3 min at 4°C again before storing on ice. The supernatant (cytoplasmic fraction, 110-120 µl) was collected and clarified by centrifugation at 18,000 ***g*** for 10 min at 4°C. Most (100 µl) of the clarified supernatant was added to 20 µl 6× Laemmli Sample Buffer (Bio-Rad), and the nuclear pellet was added to 120 µl of 1× Laemmli Sample Buffer. Samples were boiled for 6 min at 95°C. Both fractions were loaded and separated by 10% or 13% SDS-PAGE, blotted onto PVDF membranes and probed with primary and secondary antibodies, as follows: anti-histone H3 (1:2000; DSHB, ab1791; nuclear marker), anti-beta-tubulin (1:1000, DSHB, clone EP1332Y; cytoplasmic marker), rabbit anti-Wh antibody (1:2000, see above), horseradish peroxidase (HRP)-conjugated goat anti-rabbit IgG (1:5000, Jackson ImmunoResearch, 111-035-003) and HRP-conjugated goat anti-mouse IgG (1:5000, Millipore, AP124P). The blot was developed using a chemiluminescent reaction (Amersham ECL) following the manufacturer's instructions.

Development (2020) 147, dev182063. doi:10.1242/dev.182063

RNA and MicroRNA qRT-PCR

Dissected ovaries were frozen by immersion in liquid nitrogen and stored at −80°C until use. Total RNA was extracted using a standard Trizol (Ambion) extraction protocol (Su et al., 2018). In brief, 10-20 pairs of frozen ovaries were homogenized in 500 µl of Trizol, followed by a phase separation step with 500 µl 1-bromo-3-chloropropane (Sigma-Aldrich). RNA was precipitated with 500 µl isopropanol, washed with 75% ethanol, and resuspended in 30 µl RNase-free water. Genomic contamination was removed using TURBO™ DNase (Invitrogen, AM2238), according to the manufacturer's instructions for complete DNA digestion. A phenol/chloroform extraction was performed to inactivate TURBO™ DNase. MicroRNA levels were quantified using the TaqMan® MicroRNA Assay kit (Applied Biosystems, 4440885), following the manufacturer's instructions. In brief, 10 ng RNA were reversed transcribed using master mix to generate specific cDNA for each targeted microRNA, with primer sets designed from Applied Biosystems. snoRNA227 was used as a control reaction. The cDNAs were then mixed with a small RNA assay buffer containing designed primers/probes specific for each cDNA sample (Applied Biosystems) and TaqMan® Universal PCR Master Mix II (Applied Biosystems) for PCR reaction. The TaqMan™ microRNA assay miRBase ID and assay ID used in this study are listed in Table S2.

Immunoprecipitation using *Drosophila* ovaries

Frozen adult ovaries (400-600 pairs) were lysed in 300-350 µl of EB1 buffer [10 mM Hepes (pH 7.5), 10 mM KCl, 0.1% Nonidet P40, 1.5 mM $MgCl_2$, 0.2% Triton X-100] plus protease inhibitor mixture (cOmplete™, Sigma-Aldrich). After centrifugation (16,100 ***g***, 10 min at 4°C), an equal volume of EB2 buffer [20 mM Hepes (pH 7.5), 420 mM NaCl, 1.5 mM $MgCl_2$, 0.2 EDTA, 25% glycerol] was added to the supernatant; 10% of the supernatant volume was stored at −20°C as the input control. Next, 15 µl of GFP-Trap®_MA beads (ChromoTek) were equilibrated with 1 ml binding buffer [EB1]:[EB2]=1:1 three times and pull-down was performed using a MagJET Separation Rack (Thermo Fisher Scientific). The supernatants were incubated with 25-30 µl binding buffer containing equilibrated beads with gentle rotation at 4°C overnight. The beads were pulled down and washed three times, each for 1 min at 4°C, with binding buffer (freshly prepared) plus protease inhibitor mixture (cOmplete™, Sigma-Aldrich). Then 40 µl of 1× Laemmli Sample Buffer (Bio-Rad) was added to beads, and 20 µl of 2× Laemmli Sample Buffer was added to input. Both samples were boiled for 5 min, loaded and separated by SDS-PAGE, and analyzed using western blotting. Immunoblots were probed with rabbit anti-Wh (1:2000, see above), rabbit anti-Mei-p26 (1:200, a gift from P. Lasko), mouse anti-dMyc (1:20, a gift from P. Gallant, University of Würzburg, Germany) and rabbit anti-GFP (1:10,000, GenLab Biotech). Secondary antibodies included horseradish peroxidase (HRP)-conjugated goat anti-rabbit IgG (1:5000, Jackson ImmunoResearch, 111-035-003) and HRP-conjugated goat anti-mouse IgG (1:5000, Millipore, AP124P).

Immunoprecipitation using human cells

We transfected 1×10^6 293T cells with 15 µg empty vector (CMV-TRIM32-FLAG) or CMV-TRIM32-FLAG Plus CMV-WDR4-dmyc with the calcium phosphate method (the 293T cell line has recently been authenticated and has been routinely tested for free of mycoplasma contamination). Co-immunoprecipitation (co-IP) was carried out 24 h after plasmid transfection. Cells were harvested and washed with 5 ml ice-cold PBS. Then, 500 µl cold lysis buffer (0.75% NP40, 1 mM DTT in PBS) containing 1 mM phenylmethylsulphonyl fluoride (PMSF), 1 µg/ml aprotinin and 1 µg/ml leupeptin was added, and the cells were removed using a cell scraper. The mixtures were then collected and centrifuged at 13,000 rpm (15,871 ***g***) for 15 min at 4°C. We supplemented 2 mg of total protein with co-IP lysis buffer to make a total 900 µl volume, and 100 µl M2 magnetic beads (Sigma-Aldrich) was added to the sample and mixed at 4°C for 2 h. The beads were collected by centrifugation at 5000 rpm (2348 ***g***) for 1 min at 4°C. The protein-bead complexes were washed with 800 µl of co-IP lysis buffer five times. The protein-bead complexes were then denatured by heating at 95°C for 5-10 min in the presence of 1× loading buffer, which consisted of 6× loading buffer with co-IP lysis buffer. Equal amounts of samples were loaded into 10% Tris-glycine PAGE followed by SDS electrophoresis and immunoblotting.

Immunoprecipitation RT-PCR

IP was used in combination with RT-PCR as previously described (Li et al., 2012), with some modifications. In brief, 60-90 pairs of 7-day-old wild-type and wh^7 ovaries were extracted in 300 µl lysis buffer [50 mM Tris-HCl (pH 8.0), 150 mM NaCl, 0.1% Nonidet P40, 5 mM EDTA, 5 mM DTT]. Protease inhibitor mixture (cOmplete™, Sigma-Aldrich) and RNase inhibitor (40 U/µl; Roche) were added to the lysate. Supernatant was obtained by centrifugation (16,100 ***g***, 10 min at 4°C). Mouse anti-IgG Ab (1:250, Santa Cruz Biotechnology, sc-2025) or mouse anti-Sxl Ab (1:35, DSHB, M1114) was added and the samples were incubated at 4°C for 3 h. Then, the ovary lysate with antibody was incubated with pre-equilibrated Protein G Sepharose Fast Flow beads (GE Healthcare) at 4°C overnight. Beads were pelleted by centrifugation at 12,000 ***g*** for 1 min and washed briefly with 1 ml of fresh lysis buffer. Genomic DNA was removed using TURBO™ DNAase, according to the manufacturer's manual. RNA was extracted from beads by Trizol, and cDNA was made as described above. cDNA was synthesized from total RNA (100 ng) from whole ovaries and used as the template. Thirty cycles of PCR using Phusion® High-Fidelity DNA Polymerase (New England Biolabs) were performed on 1 µl of cDNA to amplify *nos* 3′ UTR using the primers listed in Table S1; the resulting products were analyzed on 1% agarose gels.

RNA and microRNA sequencing analysis

For RNA sequencing analysis, thirty pairs of ovaries were collected and dissected from 7-day-old $nos>gfp^{RNAi}$, $nos>wh^{RNAi}$, w^{1118} and wh^7 mutant flies. $nos>gfp^{RNAi}$ and $nos>wh^{RNAi}$ flies were cultured at 29°C throughout development. The analysis was performed in duplicate. Total RNA was extracted and measured by absorbance at 260 nm using an ND-1000 spectrophotometer (Nanodrop Technology). RNA quality was evaluated using a Bioanalyzer 2100 (Agilent Technology) with an RNA 6000 labchip kit (Agilent Technology). All values, $OD_{260/280}$ and $OD_{260/230}$ were above 2.15. All RNA-seq procedures were performed in accordance with the manufacturer's instructions (Illumina). The library was constructed with Agilent's SureSelect Strand Specific RNA library Preparation Kit for 75SE (Paired-End) sequencing on a Solexa platform. Sequencing-by-synthesis technology with a TruSeq SBS kit was used for the sequencing. Raw sequences were obtained from the Illumina Pipeline software bcl2fastq v2.0 and expected to generate 12.5 million reads (M) per sample. Trimmomatic software was implemented to trim or filter the reads according to the quality score. The gene expression level was calculated as fragment per kb of transcript per million mapped reads (FPKM). CummeRbund was used to perform statistical analysis of gene expression profiles for differential expression analysis. The reference gene annotations were retrieved from Flybase. For microRNA sequencing analysis, thirty pairs of ovaries were collected and dissected from 7-day-old, w^{1118}, *mei-p26* and wh^7 mutant flies and cultured at 29°C throughout developmental stages. The analysis was performed in duplicate. RNA quantity and quality were evaluated as mentioned above. All values for $OD_{260/280}$ and $OD_{260/230}$ were above 2.1. Sample libraries were prepared using the QIAseq miRNA Library kit (Qiagen) according to the manufacturer's protocol. Adaptors were ligated sequentially to the 3′ and 5′ ends of miRNAs. Subsequently, universal cDNA synthesis with UMI assignment, cDNA cleanup, library amplification and library cleanup were performed. Libraries were sequenced on an Illumina instrument (75-cycle single-end read, 75SE) and expected to generate 10M per sample. Sequencing data was processed using the Illumina software BCL2FASTQ V2.20 for small RNA sequencing analysis. Initially, the generated sequences went through a filtering process to obtain qualified reads. Trimmomatic was implemented to clip the 3′ adaptor sequence, trim or remove the reads according to the quality score and discard trimmed reads in the range of (22-35) nucleotides. Qualified reads after filtering low-quality data were analyzed using miRDeep2 software for aligning reads to the mirBase 21 database. Notably, the ovaries contained a highly abundant 30 nt rRNA fragment (the 2S rRNA), which masked the microRNA and limited analysis to only 2% of total microRNAs, similar to a previous report (Fowler et al., 2018). Gene expression level was calculated as FPKM. Heatmaps were generated by the color-scale method using Excel.

Acknowledgements
We would like to thank A. Spradling, P. Lasko, J.M. Abram, M. Buszczak, H.W. Pi, C.Y. Lee, R.S. Hawley, E. Laufer, J. Knoblich and K.H. Nakamura, for providing flies and antibodies. We also thank the Bloomington *Drosophila* Stock Center (National Institute of Health, P40OD018537), Fly Stocks of National Institute of Genetics, the Vienna *Drosophila* RNAi Center and the Developmental Studies Hybridoma Bank for *Drosophila* stocks and antibodies. We also thank J.-R. Huynh for the valuable discussion and M. Calkins for English editing.

Competing interests
The authors declare no competing or financial interests.

Author contributions
Conceptualization: H.-J.H.; Methodology: E.R., K.K., F.H., R.-H.C.; Formal analysis: E.R.; Investigation: E.R., B.-S.T., H.-J.H.; Writing - original draft: E.R., H.-J.H.; Writing - review & editing: H.-J.H.; Supervision: T.-S.H., H.-J.H.

Funding
This study was supported by intramural funding from the Institute of Cellular and Organismic Biology, Academia Sinica, Taiwan, and a thematic grant from the Academia Sinica.

Data availability
RNA sequencing and microRNA sequencing data have been deposited in GEO under accession numbers GSE142829 and GSE142830, respectively.

Supplementary information
Supplementary information available online at
http://dev.biologists.org/lookup/doi/10.1242/dev.182063.supplemental

References

Alexandrov, A., Martzen, M. R. and Phizicky, E. M. (2002). Two proteins that form a complex are required for 7-methylguanosine modification of yeast tRNA. *RNA* **8**, 1253-1266. doi:10.1017/S1355838202024019

Arama, E., Dickman, D., Kimchie, Z., Shearn, A. and Lev, Z. (2000). Mutations in the β-propeller domain of the Drosophila brain tumor (brat) protein induce neoplasm in the larval brain. *Oncogene* **19**, 3706. doi:10.1038/sj.onc.1203706

Chen, D. and McKearin, D. M. (2003). A discrete transcriptional silencer in the bam gene determines asymmetric division of the Drosophila germline stem cell. *Development* **130**, 1159-1170. doi:10.1242/dev.00325

Chen, G., Kong, J., Tucker-Burden, C., Anand, M., Rong, Y., Rahman, F., Moreno, C. S., Van Meir, E. G., Hadjipanayis, C. G. and Brat, D. J. (2014). Human Brat ortholog TRIM3 is a tumor suppressor that regulates asymmetric cell division in glioblastoma. *Cancer Res.* **74**, 4536-4548. doi:10.1158/0008-5472.CAN-13-3703

Cheng, I.-C., Chen, B. C., Shuai, H.-H., Chien, F.-C., Chen, P. and Hsieh, T.-S. (2016). Wuho is a new member in maintaining genome stability through its interaction with Flap Endonuclease 1. *PLoS Biol.* **14**, e1002349. doi:10.1371/journal.pbio.1002349

Donati, G., Montanaro, L. and Derenzini, M. (2012). Ribosome biogenesis and control of cell proliferation: p53 is not alone. *Cancer Res.* **72**, 1602-1607. doi:10.1158/0008-5472.CAN-11-3992

Eikenes, A. H., Malerød, L., Christensen, A. L., Steen, C. B., Mathieu, J., Nezis, I. P., Liestøl, K., Huynh, J.-R., Stenmark, H. and Haglund, K. (2015). ALIX and ESCRT-III coordinately control cytokinetic abscission during germline stem cell division in vivo. *PLoS Genet.* **11**, e1004904. doi:10.1371/journal.pgen.1004904

Ferreira, A., Boulan, L., Perez, L. and Milán, M. (2014). Mei-P26 mediates tissue-specific responses to the Brat tumor suppressor and the dMyc proto-oncogene in Drosophila. *Genetics* **198**, 249-258. doi:10.1534/genetics.114.167502

Fomproix, N., Gebrane-Younes, J. and Hernandez-Verdun, D. (1998). Effects of anti-fibrillarin antibodies on building of functional nucleoli at the end of mitosis. *J. Cell Sci.* **111**, 359-372. doi:10.1016/s0248-4900(98)80063-4

Fowler, E. K., Mohorianu, I., Smith, D. T., Dalmay, T. and Chapman, T. (2018). Small RNA populations revealed by blocking rRNA fragments in Drosophila melanogaster reproductive tissues. *PLoS ONE* **13**, e0191966. doi:10.1371/journal.pone.0191966

Grewal, S. S., Li, L., Orian, A., Eisenman, R. N. and Edgar, B. A. (2005). Myc-dependent regulation of ribosomal RNA synthesis during Drosophila development. *Nat. Cell Biol.* **7**, 295. doi:10.1038/ncb1223

Hannezo, E., Prost, J. and Joanny, J.-F. (2014). Growth, homeostatic regulation and stem cell dynamics in tissues. *J. R. Soc. Interface* **11**, 20130895. doi:10.1098/rsif.2013.0895

Harris, R. E., Pargett, M., Sutcliffe, C., Umulis, D. and Ashe, H. L. (2011). Brat promotes stem cell differentiation via control of a bistable switch that restricts BMP signaling. *Dev. Cell* **20**, 72-83. doi:10.1016/j.devcel.2010.11.019

Hsu, H.-J. and Drummond-Barbosa, D. (2009). Insulin levels control female germline stem cell maintenance via the niche in Drosophila. *Proc. Natl Acad. Sci. USA* **106**, 1117-1121. doi:10.1073/pnas.0809144106

Hsu, H.-J., LaFever, L. and Drummond-Barbosa, D. (2008). Diet controls normal and tumorous germline stem cells via insulin-dependent and -independent mechanisms in Drosophila. *Dev. Biol.* **313**, 700-712. doi:10.1016/j.ydbio.2007.11.006

Hughes, S. E., Miller, D. E., Miller, A. L. and Hawley, R. S. (2018). Female meiosis: synapsis, recombination, and segregation in Drosophila melanogaster. *Genetics* **208**, 875-908. doi:10.1534/genetics.117.300081

Jang, J. K., Sherizen, D. E., Bhagat, R., Manheim, E. A. and McKim, K. S. (2003). Relationship of DNA double-strand breaks to synapsis in *Drosophila*. *J. Cell Sci.* **116**, 3069. doi:10.1242/jcs.00614

Jörg, D. J., Kitadate, Y., Yoshida, S. and Simons, B. D. (2019). Competition for stem cell fate determinants as a mechanism for tissue homeostasis. *arXiv* preprint arXiv:1901.03903.

Kai, T., Williams, D. and Spradling, A. C. (2005). The expression profile of purified Drosophila germline stem cells. *Dev. Biol.* **283**, 486-502. doi:10.1016/j.ydbio.2005.04.018

Kao, S.-H., Tseng, C.-Y., Wan, C.-L., Su, Y.-H., Hsieh, C.-C., Pi, H. and Hsu, H.-J. (2015). Aging and insulin signaling differentially control normal and tumorous germline stem cells. *Aging Cell* **14**, 25-34. doi:10.1111/acel.12288

Khodjakov, A. and Rieder, C. L. (1999). The sudden recruitment of gamma-tubulin to the centrosome at the onset of mitosis and its dynamic exchange throughout the cell cycle, do not require microtubules. *J. Cell Biol.* **146**, 585-596. doi:10.1083/jcb.146.3.585

Kuo, L. J. and Yang, L.-X. (2008). γ-H2AX-a novel biomarker for DNA double-strand breaks. *In Vivo* **22**, 305-309.

Lake, C. M., Holsclaw, J. K., Bellendir, S. P., Sekelsky, J. and Hawley, R. S. (2013). The development of a monoclonal antibody recognizing the Drosophila melanogaster phosphorylated histone H2A variant (γ-H2AV). *G3*, **3**, 1539-1543. doi:10.1534/g3.113.006833

Lantz, V., Chang, J. S., Horabin, J. I., Bopp, D. and Schedl, P. (1994). The Drosophila orb RNA-binding protein is required for the formation of the egg chamber and establishment of polarity. *Genes Dev.* **8**, 598-613. doi:10.1101/gad.8.5.598

Li, Y., Minor, N. T., Park, J. K., McKearin, D. M. and Maines, J. Z. (2009). Bam and Bgcn antagonize Nanos-dependent germ-line stem cell maintenance. *Proc. Natl. Acad. Sci. USA* **106**, 9304-9309. doi:10.1073/pnas.0901452106

Li, Y., Maines, J. Z., Tastan, Ö. Y., McKearin, D. M. and Buszczak, M. (2012). Mei-P26 regulates the maintenance of ovarian germline stem cells by promoting BMP signaling. *Development* **139**, 1547-1556. doi:10.1242/dev.077412

Li, Y., Zhang, Q., Carreira-Rosario, A., Maines, J. Z., McKearin, D. M. and Buszczak, M. (2013). Mei-P26 cooperates with Bam, Bgcn and Sxl to promote early germline development in the Drosophila ovary. *PLoS ONE* **8**, e58301. doi:10.1371/journal.pone.0058301

Lin, H. and Spradling, A. C. (1993). Germline stem cell division and egg chamber development in transplanted Drosophila germaria. *Dev. Biol.* **159**, 140-152. doi:10.1006/dbio.1993.1228

Lin, H., Yue, L. and Spradling, A. C. (1994). The Drosophila fusome, a germline-specific organelle, contains membrane skeletal proteins and functions in cyst formation. *Development* **120**, 947-956.

Manheim, E. A. and McKim, K. S. (2003). The Synaptonemal complex component C(2)M regulates meiotic crossing over in Drosophila. *Curr. Biol.* **13**, 276-285. doi:10.1016/S0960-9822(03)00050-2

Mathieu, J., Cauvin, C., Moch, C., Radford, S. J., Sampaio, P., Perdigoto, C. N., Schweisguth, F., Bardin, A. J., Sunkel, C. E., McKim, K. et al. (2013). Aurora B and cyclin B have opposite effects on the timing of cytokinesis abscission in Drosophila germ cells and in vertebrate somatic cells. *Dev. Cell* **26**, 250-265. doi:10.1016/j.devcel.2013.07.005

Matias, N. R., Mathieu, J. and Huynh, J.-R. (2015). Abscission is regulated by the ESCRT-III protein shrub in Drosophila germline stem cells. *PLoS Genet.* **11**, e1004653. doi:10.1371/journal.pgen.1004653

McKearin, D. (1997). The Drosophila fusome, organelle biogenesis and germ cell differentiation: if you build it? *BioEssays* **19**, 147-152. doi:10.1002/bies.950190209

McKearin, D. and Ohlstein, B. (1995). A role for the Drosophila bag-of-marbles protein in the differentiation of cystoblasts from germline stem cells. *Development* **121**, 2937.

Nähse, V., Christ, L., Stenmark, H. and Campsteijn, C. (2017). The abscission checkpoint: making it to the final cut. *Trends Cell Biol.* **27**, 1-11. doi:10.1016/j.tcb.2016.10.001

Nakada, D., Levi, B. P. and Morrison, S. J. (2011). Integrating physiological regulation with stem cell and tissue homeostasis. *Neuron* **70**, 703-718. doi:10.1016/j.neuron.2011.05.011

Neumüller, R. A., Betschinger, J., Fischer, A., Bushati, N., Poernbacher, I., Mechtler, K., Cohen, S. M. and Knoblich, J. A. (2008). Mei-P26 regulates microRNAs and cell growth in the Drosophila ovarian stem cell lineage. *Nature* **454**, 241. doi:10.1038/nature07014

Ohlstein, B. and McKearin, D. (1997). Ectopic expression of the Drosophila Bam protein eliminates oogenic germline stem cells. *Development* **124**, 3651.
Page, S. L. and Hawley, R. S. (2001). c(3)G encodes a Drosophila synaptonemal complex protein. *Genes Dev.* **15**, 3130-3143. doi:10.1101/gad.935001
Page, S. L., McKim, K. S., Deneen, B., Van Hook, T. L. and Hawley, R. S. (2000). Genetic studies of mei-P26 reveal a link between the processes that control germ cell proliferation in both sexes and those that control meiotic exchange in Drosophila. *Genetics* **155**, 1757.
Pierce, S. B., Yost, C., Britton, J. S., Loo, L. W. M., Flynn, E. M., Edgar, B. A. and Eisenman, R. N. (2004). dMyc is required for larval growth and endoreplication in Drosophila. *Development* **131**, 2317. doi:10.1242/dev.01108
Rørth, P. (1998). Gal4 in the Drosophila female germline. *Mech. Dev.* **78**, 113-118. doi:10.1016/S0925-4773(98)00157-9
Rudra, D. and Warner, J. R. (2004). What better measure than ribosome synthesis? *Genes Dev.* **18**, 2431-2436. doi:10.1101/gad.1256704
Sanchez, C. G., Teixeira, F. K., Czech, B., Preall, J. B., Zamparini, A. L., Seifert, J. R. K., Malone, C. D., Hannon, G. J. and Lehmann, R. (2016). Regulation of ribosome biogenesis and protein synthesis controls germline stem cell differentiation. *Cell Stem Cell* **18**, 276-290. doi:10.1016/j.stem.2015.11.004
Sardiello, M., Cairo, S., Fontanella, B., Ballabio, A. and Meroni, G. (2008). Genomic analysis of the TRIM family reveals two groups of genes with distinct evolutionary properties. *BMC Evol. Biol.* **8**, 225. doi:10.1186/1471-2148-8-225
Schapira, M., Tyers, M., Torrent, M. and Arrowsmith, C. H. (2017). WD40 repeat domain proteins: a novel target class? *Nat. Rev. Drug Discov.* **16**, 773-786. doi:10.1038/nrd.2017.179
Sekelsky, J. J., McKim, K. S., Messina, L., French, R. L., Hurley, W. D., Arbel, T., Chin, G. M., Deneen, B., Force, S. J., Hari, K. L. et al. (1999). Identification of novel Drosophila meiotic genes recovered in a P-element screen. *Genetics* **152**, 529.
Simons, B. D. and Clevers, H. (2011). Strategies for homeostatic stem cell self-renewal in adult tissues. *Cell* **145**, 851-862. doi:10.1016/j.cell.2011.05.033
Song, X., Wong, M. D., Kawase, E., Xi, R., Ding, B. C., McCarthy, J. J. and Xie, T. (2004). Bmp signals from niche cells directly repress transcription of a differentiation-promoting gene, bag of marbles, in germline stem cells in the Drosophila ovary. *Development* **131**, 1353-1364. doi:10.1242/dev.01026
Spradling, A. C. and Rubin, G. M. (1982). Transposition of cloned P elements into Drosophila germ line chromosomes. *Science* **218**, 341. doi:10.1126/science.6289435
Spradling, A., Fuller, M. T., Braun, R. E. and Yoshida, S. (2011). Germline stem cells. *Cold Spring Harbor Perspect. Biol.* **3**, a002642. doi:10.1101/cshperspect.a002642
Stirnimann, C. U., Petsalaki, E., Russell, R. B. and Müller, C. W. (2010). WD40 proteins propel cellular networks. *Trends Biochem. Sci.* **35**, 565-574. doi:10.1016/j.tibs.2010.04.003
Storto, P. D. and King, R. C. (1989). The role of polyfusomes in generating branched chains of cystocytes during Drosophila oogenesis. *Dev. Genet.* **10**, 70-86. doi:10.1002/dvg.1020100203
Su, Y.-H., Rastegri, E., Kao, S.-H., Lai, C.-M., Lin, K.-Y., Liao, H.-Y., Wang, M.-H. and Hsu, H.-J. (2018). Diet regulates membrane extension and survival of niche escort cells for germline homeostasis via insulin signaling. *Development* **145**, dev159186. doi:10.1242/dev.159186
Tocchini, C. and Ciosk, R. (2015). TRIM-NHL proteins in development and disease. *Semin. Cell Dev. Biol.* **47-48**, 52-59. doi:10.1016/j.semcdb.2015.10.017
Tseng, C.-Y., Su, Y.-H., Yang, S.-M., Lin, K.-Y., Lai, C.-M., Rastegari, E., Amartuvshin, O., Cho, Y., Cai, Y. and Hsu, H.-J. (2018). Smad-independent BMP signaling in somatic cells limits the size of the germline stem cell pool. *Stem Cell Rep.* **11**, 811-827. doi:10.1016/j.stemcr.2018.07.008
van Riggelen, J., Yetil, A. and Felsher, D. W. (2010). MYC as a regulator of ribosome biogenesis and protein synthesis. *Nat. Rev. Cancer* **10**, 301-309. doi:10.1038/nrc2819
Wang, Z. and Lin, H. (2004). Nanos maintains germline stem cell self-renewal by preventing differentiation. *Science* **303**, 2016. doi:10.1126/science.1093983
Wang, Y.-T., Chen, J., Chang, C.-W., Jen, J., Huang, T.-Y., Chen, C.-M., Shen, R., Liang, S.-Y., Cheng, I.-C., Yang, S.-C. et al. (2017). Ubiquitination of tumor suppressor PML regulates prometastatic and immunosuppressive tumor microenvironment. *J. Clin. Invest.* **127**, 2982-2997. doi:10.1172/JCI89957
Wettstein, R. and Sotelo, J. (1971). The molecular architecture of synaptonemal complexes. *Adv. Cell Mol. Biol* **1**, 109-152.
White-Cooper, H. and Caporilli, S. (2013). Transcriptional and post-transcriptional regulation of Drosophila germline stem cells and their differentiating progeny. *Transcript. Transl. Regul. Stem Cells* **786**, 47-61. doi:10.1007/978-94-007-6621-1_4
Wong, M. D., Jin, Z. and Xie, T. (2005). Molecular mechanisms of germline stem cell regulation. *Annu. Rev. Genet.* **39**, 173-195. doi:10.1146/annurev.genet.39.073003.105855
Wu, J., Hou, J. H. and Hsieh, T.-S. (2006). A new Drosophila gene wh (wuho) with WD40 repeats is essential for spermatogenesis and has maximal expression in hub cells. *Dev. Biol.* **296**, 219-230. doi:10.1016/j.ydbio.2006.04.459
Wylie, A., Lu, W.-J., D'Brot, A., Buszczak, M. and Abrams, J. M. (2014). p53 activity is selectively licensed in the Drosophila stem cell compartment. *eLife* **3**, e01530-e01530. doi:10.7554/eLife.01530
Xu, C. and Min, J. (2011). Structure and function of WD40 domain proteins. *Protein Cell* **2**, 202-214. doi:10.1007/s13238-011-1018-1
Xu, T. and Rubin, G. M. (1993). Analysis of genetic mosaics in developing and adult Drosophila tissues. *Development* **117**, 1223.
Zaccai, M. and Lipshitz, H. D. (1996). Role of Adducin-like (hu-li tai shao) mRNA and protein localization in regulating cytoskeletal structure and function during Drosophila oogenesis and early embryogenesis. *Dev. Genet.* **19**, 249-257. doi:10.1002/(SICI)1520-6408(1996)19:3<249::AID-DVG8>3.0.CO;2-9